RESEARCH ARTICLE

INTERNATIONAL RESEARCH JOURNAL OF MULTIDISCIPLINARY TECHNOVATION

Asian Research Association

DOI: 10.54392/irjmt2634

From Champion Cells to Bankable Modules: Stability, Scalable Manufacturing, and Standardized Reliability Testing for Perovskite Photovoltaics

B. Punithaveni [a, *], D. Nithyaprakash [b], Mohanbabu Bharathi [b, c, *]

[a] Department of Physics, PSGR Krishnammal College for Women, Coimbatore, Tamil Nadu, India
[b] Department of Physics, PPG Institute of Technology, Coimbatore, Tamil Nadu, India
[c] Centre for Research Impact & Outcome, Chitkara University, Rajpura, 140401, Punjab, India
* Corresponding Author's Email: punithip12@gmail.com, mohanbabuedu@gmail.com

DOI: https://doi.org/10.54392/irjmt2634
Received: 05-02-2026; Revised: 20-04-2026; Accepted: 29-04-2026; Published: 04-05-2026

Abstract: Metal halide perovskite solar cells have experienced unprecedented growth over the last fifteen years. The certified single-junction efficiency has now reached 26.95%, while perovskite-silicon tandems have already exceeded the practical Shockley-Queisser limit by achieving efficiencies above 34.6%, as confirmed by certified measurements. Nevertheless, bankable perovskite modules are still lacking. The central challenge is no longer simply material degradation, but the absence of a validated approach that links laboratory performance metrics, such as power conversion efficiency in small-area cells or ISOS L-1 T80 lifetime, to certified performance metrics, such as power conversion efficiency in large-area cells, which must be statistically reproducible and IEC-qualified before they can be accepted by financiers and independent engineers in decision-making processes. This work addresses that gap by introducing a qualification-oriented analytical framework. A systematic literature search was conducted on peer-reviewed papers published between 2018 and 2025 using databases such as Web of Science, Scopus, and ScienceDirect, with keywords related to perovskite solar cell efficiencies, ISOS L-1 stability, IEC qualification, encapsulation, scalable deposition techniques, and techno-economic studies. Only papers in which test conditions, active area, and encapsulation state were clearly defined were included in the review. Device-level and module-level data were treated as distinct types of evidence. Separate tables are provided for certified performance, operational stability, qualification-relevant module tests, and techno-economic studies to avoid misleading comparisons between different evidence types. A four-domain translation framework is introduced to connect efficiency, degradation physics, engineering readiness, and financial bankability within an analytical structure that includes explicit cross-domain dependencies. To standardise comparison across research groups and pilot-scale demonstrations, a composite Perovskite Module Readiness Index is proposed. The analysis also defines the critical validation milestones that must be achieved before commercially viable implementation and outlines the baseline technical evidence needed to support bankability assessments.

Keywords: Perovskite Solar Cells, Module Stability, Scalable Deposition, Encapsulation, ISOS Protocols, IEC Qualification, Bankability, Tandem Photovoltaics, Ion Migration, T80/T90 Lifetime.

1. Introduction

Metal halide perovskite solar cells have progressed faster than any other photovoltaic technology in recorded history [1]. In 2009, organometal halide perovskites were first demonstrated as visible-light sensitisers in photovoltaic devices, reporting a power conversion efficiency of 3.8% [2]. Within fifteen years, Certified single-junction efficiency reached 26.95%, as reported in the NREL Best Research-Cell Efficiency Chart (Solar Cell Efficiency Tables, Version 66) [3], and perovskite-silicon tandem devices crossed 34.6% certified efficiency [4]. These values exceed the practical efficiency limit of single-junction silicon defined by the Shockley–Queisser framework. The photovoltaic potential of perovskite materials is therefore clearly established. However, this efficiency progress has not yet translated into products that the photovoltaic industry, project financiers, and independent engineers will accept as commercially viable. The concept of bankability has a precise technical meaning in the photovoltaic industry. The concept of bankability, as defined in photovoltaic financial risk assessment

literature [5], refers to its long-term energy yield with actuarial confidence over a project life of 20 to 35 years.

This confidence depends on certified power measurements based on aperture area, independently validated stability under IEC 61215 and IEC 61730 qualification sequences, outdoor field data with statistically supported degradation rates, and warranty backing from financially stable manufacturers. It took 20 years of work and many reliability failures before crystalline silicon met this standard. Perovskite technology is progressing rapidly; however, the comprehensive evidence package required for financial endorsement is still lacking in most published reports [6]. Stability studies conducted in accordance with IEC 61215 have clearly delineated the existing gap between current laboratory demonstrations and formal qualification criteria [6].

Several reviews have addressed individual dimensions of this challenge. Some focus on degradation mechanisms in single-junction cells [7], others on encapsulation strategies [8], on tandem integration [9], or on scalable deposition processes [10]. No previous review has created a single, analytically structured translation framework that connects efficiency scaling, degradation physics, qualification logic, and financial risk into one predictive pathway. Table 1 compares the range of representative previous reviews to the framework suggested in this paper. The unaddressed gap is the lack of a systems-level connection from laboratory metrics, like small-area power conversion efficiency and ISOS-L-1 T80, to bankable module performance, which is defined as IEC-qualified durability, statistically reproducible manufacturing yield, and warranty-compatible annual degradation rates below 1% [11].

A four-domain translation framework has been constructed to formalise this process. The first domain deals with efficiency scaling losses, while the second focuses on degradation mechanisms and stressor interactions. Engineering solutions, such as interconnection design and encapsulation techniques, are included in the third domain. The fourth domain considers broader techno-economic drivers, warranty structures, and financial bankability thresholds. Crucially, this translation framework serves as an operational model for cross-domain decision-making and goes beyond a purely descriptive role.

The translation framework is useful only if the four domains remain linked through explicitly defined analytical relationships, as described in Section 1.3. Section 9 introduces the Perovskite Module Readiness Index, which converts this translation scheme into a single metric and operationalises the framework. The review also outlines the minimum data package required for assessment by a financier or independent engineer in the event of a warranty claim.

1.1 Comparative Positioning of Existing Reviews and Novel Contribution

A direct comparison with the existing body of perovskite review literature is necessary to establish the novelty of this review. Previous reviews can be grouped into five main themes. The first category includes cell-level instability studies, such as the work of Duan *et al.* [7], which analyses photochemical stabilization pathways at the device level but does not discuss module-level interconnect losses, manufacturing yield, or financial risk. The second category focuses on encapsulation and environmental sealing strategies. Dipta *et al.* investigated lead containment and moisture barriers [8]. The third category concerns tandem-device integration [9]. It presents certified efficiency milestones and architecture comparisons, but it does not translate these advances into financial risk metrics or bankability thresholds. The fourth category covers scalable manufacturing and process development [10], evaluating deposition methods and pilot-line progress without systematically linking process-yield statistics to degradation-informed lifetime models. The fifth category comprises qualification-focused reviews [6], which examine IEC protocol gaps but do not extend the analysis to financial warranty structures or investment risk.

The current review offers a four-domain analytical framework that none of the preceding studies provides, either separately or collectively. It makes three specific contributions that are not found in the existing review literature. First, it establishes clear cross-domain dependencies: the efficiency domain constrains the financial domain through module-level aperture efficiency targets; the degradation domain constrains the engineering domain through encapsulation WVTR requirements; and the qualification domain constrains the financial domain through warranty-compatible degradation-rate thresholds. Second, it separates evidence by class, treating certified performance, operational stability, qualification-relevant module tests, and techno-economic studies as separate datasets rather than combining them in a single comparison table. Third, it introduces a composite readiness metric, the Perovskite Module Readiness Index, that operationalises the transition from research demonstration to a bankable product. These distinctions are summarised in Table 1.

1.2 Standardised Terminology

To compare findings from different studies, several definitions are necessary. Inconsistent terminology creates confusion and also permits exaggerated efficiency claims. The definitions of the key terms used in this review are listed in Table 2.

Table 1. Scope Comparison of Representative Perovskite Review Articles Against the Present Framework

Reference	Efficiency & Scaling	Degradation Physics	Qualification Logic	Financial Risk	Cross-Domain Analytical Links
[6]	No	Yes	Yes	No	No
[7]	Limited	Yes	No	No	No
[8]	No	Yes	Yes	No	No
[9]	Yes	Yes	No	No	No
[10]	Yes	Limited	No	No	No
Present review	Yes	Yes	Yes	Yes	Yes (explicit)

Table 2. Standardised Area and Stability Definitions for Perovskite Photovoltaic Devices and Modules

Term	Definition	Measurement Basis	Relevance to Bankability
Cell area	Total physical substrate area of a photovoltaic device, including active region, contact pads, and non-illuminated regions.	Measured geometrically from device layout; includes all patterned regions.	Overestimation of performance may occur if efficiency is reported using smaller active or aperture areas without disclosure.
Active area	Area of the device that contains the functional photovoltaic junction and contributes to photocurrent generation.	Typically defined by mask during J–V measurement or photolithographic patterning.	Enables fair comparison of intrinsic device efficiency; however, does not reflect module-scale interconnect losses.
Aperture area	Illuminated area exposed to simulated or natural sunlight during measurement.	Defined by calibrated shadow mask during performance testing under standard test conditions (STC).	Certified module efficiencies for bankability must be based on aperture area greater than 100 cm^2.
Dead area fraction	Percentage of total module area rendered inactive due to laser scribing, interconnect spacing, and edge borders.	Calculated as (inactive area / total module area) × 100%.	Directly reduces geometric fill factor and module power output. Dead area above 5% undermines economic viability.
T80 / T90	Time required for a device or module to retain 80% or 90% of its initial power conversion efficiency under defined stress conditions.	Determined under specified ISOS or IEC protocols; must state illumination mode, temperature, atmosphere, and bias condition.	Core lifetime metric used to estimate degradation rate and warranty compatibility; must be measured under MPP for financial relevance.
ISOS-L-1	Continuous one-sun illumination at open-circuit condition with periodic performance measurement.	Indoor light soaking under controlled temperature.	Useful for mechanistic comparison but underestimates degradation relative to MPP operation. Limited predictive value for warranty modelling.
ISOS-L-2	Continuous one-sun illumination with maximum power point tracking and real-time monitoring of stabilised output.	Indoor light soaking under active MPP operation.	More representative of operational stress. Preferred protocol for projecting annual degradation and assessing bankability readiness.
Area basis	The specific area definition used as the denominator for efficiency reporting.	Must be explicitly stated in every published result.	Reviewers and financiers cannot compare studies that use different area bases without disclosure.

Stability claims and efficiency reports may not be useful for financial evaluation in the absence of standardised definitions. For each comparison entry in this review, the definitions listed in Table 2 are applied uniformly.

1.3 The Four Domain Translation Framework and Cross Domain Dependencies

The cell-to-module translation problem is divided into four analytically connected domains in this review. Active-area power conversion efficiency, resistive scaling losses during area expansion, and the dead-area percentage brought about by laser scribing and connection design are all included in the Efficiency Domain. Ion migration energetics, phase instability in mixed-halide and mixed-cation systems, and the effects of combined environmental and electrical stressors under operating conditions are all covered in the Degradation Domain. Encapsulation techniques, connection design, and IEC-compliant qualification-style reliability testing are all integrated in the Engineering Domain. The Financial Domain includes explicit bankability thresholds necessary for investment confidence, statistical production yield, and deterioration warranty curves.

The four domains are interconnected. Each domain constrains the others in analytically specific ways by defining the minimum performance criteria for bankable projects. The Efficiency Domain constrains the Financial Domain, such that if aperture efficiency is below 20%, with an area greater than 100 cm², it cannot meet levelized cost of electricity targets for utility-scale project approvals, as costs are proportional to module area, not peak power [12]. The Degradation Domain constrains the Engineering Domain, such that the required rate of water vapour transmission through an encapsulant is determined by the composition of the perovskite absorber material, which is moisture-sensitive, and is limited by the maximum degradation rate, itself determined by warranty conditions in the Financial Domain [8]. The Engineering Domain constrains the Financial Domain, such that if individual stress tests are passed but sequential qualification is failed, it cannot support a bankable warranty claim, as sequential qualification is more representative of outdoor stress than individual failure modes [6, 13]. The Efficiency Domain constrains the Degradation Domain, such that increased cell pitches, to improve geometric fill factor by reducing scribe line density, also increase both lateral current flow and local joule heating, thereby accelerating ion motion and phase instability [14]. These cross-domain dependencies mean that optimising any single domain in isolation will not produce a bankable module. A translation framework must address all four domains simultaneously and define the minimum acceptable performance in each relative to the thresholds of the others. Figure 1 shows the conceptual framework of the cell-to-module translation model, with domain interdependencies indicated.

2. State of the Art and the Cell-to-Module Translation Gap

2.1. Certified Performance Landscape and Architecture Snapshot

In 2025, certified data demonstrate very high efficiency for small-area perovskite cells but considerably lower values at module scale. Solar Cell Efficiency Tables, Version 66, reports a certified efficiency of 26.95% for a halide perovskite solar cell [3]. Earlier tables reported 26.7% for a 0.05 cm² p-i-n perovskite cell in Version 64 [15] and 26.1% in Version 63 [16].

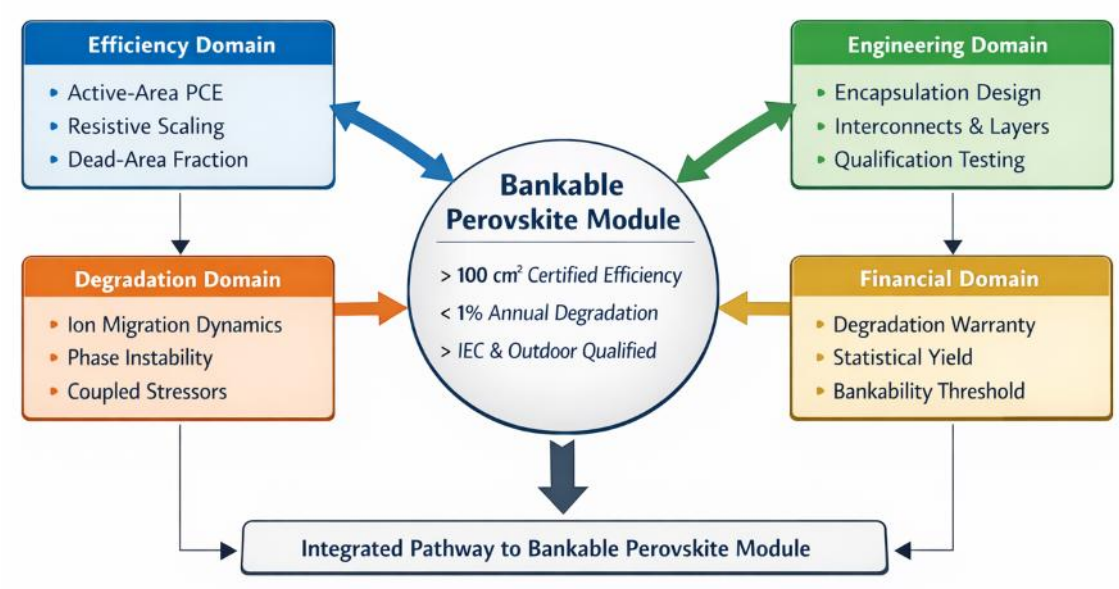

Figure 1. Conceptual framework for perovskite modules

Efficiency progression from 26.1% (Version 63) to 26.7% (Version 64) and 26.95% (Version 66) reflects incremental improvements in device passivation and interface engineering. These results confirm steady progress in device optimisation. The p-i-n architecture has gained importance because of its compatibility with low-temperature processing and reduced hysteresis, and it supports self-assembled monolayer hole contacts suitable for scalable production [17]. For perovskite-silicon tandem devices, certified efficiency has exceeded 34.6% [4]. All-perovskite tandems have reached 29.7% under laboratory conditions [9]. At module level, a 216 cm² lead-halide perovskite submodule achieved 20.6% certified efficiency [4], and a minimodule of 20 cm² with eight cells in series reached 22.6% [15]. The gap between small-area cells at approximately 27% and large modules at approximately 20-21% is therefore 6-7 percentage points for single-junction devices. This gap represents the central scale-up challenge and motivates the loss-budget analysis in Section 2.2.

2.2. Module Level Loss Budget

The efficiency difference between a laboratory cell and a commercial module arises from four distinct and quantifiable loss mechanisms. Understanding their individual contributions is essential for defining engineering priorities. The following loss decomposition is based on analytical modelling and data from representative module studies [19]. The total cell-to-module efficiency gap of approximately 6-7 percentage points can be apportioned as follows: dead-area loss from laser scribing accounts for approximately 2.5-3.5 percentage points; resistive loss from transparent conducting oxide sheet resistance accounts for approximately 1.5-2.5 percentage points; optical losses at interconnect regions account for approximately 0.5-1.0 percentage points; and processing non-uniformity over large substrates accounts for approximately 1.0-2.0 percentage points. These values represent ranges observed across published module studies and will vary with specific device architecture and process conditions.

The geometry of laser scribing determines dead-area loss. Monolithic modules define isolated subcells and join them in series using a three-step scribing sequence, P1, P2, and P3 [20]. Each laser line removes material over a width typically between 100 and 400 micrometres. For a scribe width of 300 micrometres and a cell width of 7 millimetres, the geometric fill factor is approximately 0.91, meaning that nearly 9% of the module area does not generate current. Laser damage and debris at scribe edges can also create shunts that further reduce performance. Optimised scribing can reduce total dead width below 200 micrometres, yielding geometric fill factors above 0.95, which is the target defined in Section 9. The relationship between cell width and total dead-area fraction can be expressed as,

$$Dead - area\ fraction = (n \times scribe\ width) / module\ length \quad (1)$$

Where n is the number of interconnect lines per module.

Resistive loss from transparent conducting oxide electrodes is determined by sheet resistance, cell width, and current density. For indium tin oxide with a sheet resistance of 12 ohms per square and a current density of 20 mA cm⁻², a cell width of 8 millimetres produces a fill factor loss of approximately 2-3% compared to an ideal zero-resistance case [19]. Narrower cells reduce this resistive loss but increase dead-area fraction because more scribe lines are needed. This relation defines an optimal cell width between approximately 5 and 10 millimetres for standard indium tin oxide substrates. Alternative transparent electrodes with lower sheet resistance, such as hydrogen-doped indium oxide, can shift this optimum toward wider cells and lower overall loss [21].

Optical losses arise from light absorption or reflection at metal grid connections and scribe lines. Although this contribution is smaller than resistive and dead-area losses, it becomes more important as scribing optimisation reduces mechanical dead area [22]. Processing non-uniformity is the most difficult loss mechanism to quantify because it depends on equipment, substrate size, ambient conditions, and operator skill. Fill factor can be reduced by 1-2% because of local current mismatches caused by film-thickness variations of more than 10% across a substrate. In-line metrology during deposition is the primary method for identifying and correcting these discrepancies before they propagate to the final module.

2.3. Classification Framework of Uniformity, Yield, and Reproducibility

One important and often overlooked aspect of module performance is reproducibility. Numerous papers report data from only a limited number of substrates and highlight a single high-efficiency device. Manufacturing yield above ~95% is generally required for industrial production [23–25]. This evaluation divides the available research into three groups to systematically assess repeatability. Category A studies report champion values from fewer than ten devices and do not provide batch statistics. Category B studies report the mean and standard deviation from 10 to 50 devices, although the data may still come from a single batch or substrate.

Category C studies assess the coefficient of variation across several production runs with sample sizes greater than 50 devices. Most module-efficiency reports exceeding 20% fall into Category A under this classification scheme. Category C data are still largely absent from the current literature, and only a small number of studies meet the requirements for Category

B. Tables 3–6 provide the details of these categories and organise the evidence by type and reproducibility.

The lack of Category C data directly affects bankability. Financial actuarial models require statistically validated degradation distributions rather than single-device lifetime claims. For warranty pricing, batch-variability data for power conversion efficiency, open-circuit voltage, short-circuit current, and fill factor across several production runs must show a coefficient of variation below 5%. This standard has not yet been demonstrated at scale for perovskite modules. A study on blade-coated modules suggests that careful control of interface morphology and additive chemistry may reduce efficiency fluctuations [24]. However, maintaining stable batch conditions required repeated optimisation. Bridging this repeatability gap will require a deeper understanding of nucleation and crystal growth.

2.4. Evidence Classification of Performance, Stability, Qualification and Cost Data

Evidence from different study types must be assessed independently because they cannot be directly compared. Fundamentally distinct evidence types include certified record cells, tandem devices, minimodules, stability reports, damp-heat tests, outdoor monitoring results, laser-scribing investigations, cost models, and broader review articles. Their differing levels of certainty and relevance to bankable deployment are obscured when they are combined into a single comparative dataset. Accordingly, this review presents the evidence in four separate tables. Certified performance records are included in Table 3. Active-area and aperture-area efficiencies are reported separately and should not be directly compared without correction for geometric and interconnection losses. Operational stability and lifetime studies are covered in Table 4. Qualification-relevant module tests are summarised in Table 5. Table 6 lists the techno-economic studies. T80 represents time to 80% initial efficiency, while retention values indicate remaining performance at a fixed time; these metrics are not interchangeable.

Table 3. Certified and Laboratory Performance Records for Perovskite Cells and Modules

Year	Device Type	Architecture	Area (cm²)	Area Basis	PCE (%)	Certification Status	Repro. Cat.	Reference
2025	Single-junction	p-i-n	0.06	Active	26.95	Certified (NREL)	A	[3]
2025	Tandem (Si)	2T monolithic	1.0	Aperture	34.6	Certified (NREL)	A	[4]
2025	All-perovskite tandem	2T	0.05	Active	29.7	Laboratory (Not certified)	A	[9]
2024	Single-junction	p-i-n	0.05	Active	26.7	Certified	A	[15]
2024	Minimodule	p-i-n (8-cell)	20.0	Aperture	22.6	Certified	A	[15]
2024	Single-junction	n-i-p	0.10	Active	26.1	Certified	A	[16]
2025	Submodule	29-cell series	216	Aperture	20.6	Certified	A	[4]

Table 4. Operational Stability and Lifetime Studies (Standardised ISOS Reporting with Explicit Metrics)

Year	Device / Module	Area (cm²)	ISOS Protocol	Operation Mode	Stress Condition	Metric Type	Value	Encapsulation	Ref.
2026	Perovskite-Si module	65.1	ISOS-L-2	MPP	1 sun	T80	>1000 h	Glass-glass	[25]
2024	Blade-coated module	110	ISOS-T-1	Thermal	85°C air	Retention	84% @1000 h	Encapsulated	[26]
2025	Slot-die FA-Cs module	100	ISOS-L-2	MPP	1 sun, 65% RH	Retention	94% @1000 h	Encapsulated	[27]
2024	Module (60.84 cm²)	60.84	ISOS-L-2	MPP	1 sun	T90	>1000 h	Encapsulated	[28]
2023	Carbon electrode cell	Small	ISOS-L-1	Open circuit	1 sun	T80	>2000 h	Encapsulated	[29]
2024	Outdoor minimodule	Small	ISOS-O	Outdoor	Real conditions	Qualitative	Reported	Encapsulated	[30]

Table 5. Qualification-Relevant Module Tests (IEC-Referenced)

Year	Device / Module	Area (cm²)	Test Type	Stress Condition	Retention	Qualification Status	Reference
2022	Glass-glass module	Not reported (NR)	Damp heat	85°C / 85% RH	>95% @1566 h	IEC-relevant	[31]
2024	Strain-compliant module	NR	Damp heat + TC	85°C / 85% RH; -40 to +85°C	98% @1000 h; 95% @220 cycles	Partial IEC	[32]
2024	Shellac module	NR	IEC UV + hail	Outdoor	Passed	IEC-qualified	[33]
2022	Qualification review	N/A	IEC 61215	Framework	Gap identified	Review	[6]

Table 6. Techno-Economic and Sustainability Studies

Year	Study Focus	Key Assumption	Key Outcome	Reference
2023	Single-junction LCOE model	PCE >24%, yield >95%	LCOE 2.8-9.1 ct/kWh by 2050	[34]
2025	Cost competitiveness model	20-24% PCE, 20-30 yr lifetime	Requires PCE >24% with 20-yr lifetime for European markets	[35]
2025	Tandem LCOE projection	Module PCE >30%	LCOE 10-20% lower than Si	[36]
2023	Recycling and sustainability	Glass and ITO recovery	Significant energy and material savings at end-of-life	[37]
2025	Manufacturing cost analysis	Yield 95%, scale-up	Yield loss from 95% to 85% increases cost per watt by 10-18%	[38]

Each entry includes the area basis, ISOS or IEC protocol name, stress condition, operational mode, encapsulation state, certification status, and repeatability category, following the reporting template used in this review.

3. Degradation and Failure Physics under Realistic Stressors

3.1. Degradation Pathways Ranking by Module Bankability Relevance

Numerous degradation mechanisms are discussed in the literature on perovskite solar cells, but not all are equally important for the deployment of bankable modules. This section distinguishes mechanisms that are primarily cell-level concerns from those that pose a serious risk to module bankability and ranks the major degradation processes according to their relevance to module-level durability under operating conditions. The ranking is based on the degree of efficiency loss, the reversibility of the mechanism, and the availability of engineering mitigation strategies.

For single-junction perovskite modules, the three degradation mechanisms most critical to bankability are interface degradation at the metal back contact, ion migration under operating electric fields, and moisture ingress caused by encapsulation failure. Moisture ingress is especially important because controlled laboratory humidity tests cannot fully reproduce realistic encapsulation failures, and because moisture infiltration causes rapid and largely irreversible phase degradation [39]. Ion migration is also critical because it causes gradual efficiency loss under maximum power point operation, directly affects bankable energy yield, and introduces hysteresis that complicates performance measurement [14]. Likewise, interface degradation at silver or gold contacts can increase series resistance over time in ways that are difficult to detect early and are not fully captured by single-stressor accelerated tests.

The ranking changes for tandem perovskite-silicon modules. Photoinduced halide segregation in the wide-bandgap perovskite top cell is an additional crucial process. Halide segregation under illumination creates iodide-rich and bromide-rich domains that reduce open-circuit voltage and cause progressive bandgap narrowing under sustained operation [14, 40]. This mechanism is particularly relevant for tandems because the top cell operates at high photon flux and requires a wider bandgap than single-junction optimum compositions. Tin oxidation in the narrow-bandgap subcell of all-perovskite tandems represents a further

unique pathway. Tin (II) oxidises rapidly to tin (IV) under even trace oxygen exposure, creating deep traps that degrade carrier lifetime in the Sn-Pb absorber [9]. This pathway requires more stringent encapsulation and more careful ambient processing controls than single-junction lead-only compositions.

A degradation mechanism that is frequently reported in cell-level studies but is less critical at the module bankability level is thermal decomposition of methylammonium-based compositions above 80°C. This pathway is largely mitigated in current high-efficiency formulations by the replacement of methylammonium with formamidinium and cesium cation mixtures, which raise the thermal stability threshold to above 120°C [29]. Similarly, superoxide-mediated degradation at titanium dioxide electron transport layers is a significant cell-level concern that is effectively addressed at the module level by replacing titanium dioxide with tin (IV) oxide. These mechanisms therefore have lower priority in the module bankability ranking despite their prominence in the cell-level literature.

3.2. Moisture and Oxygen Degradation

Moisture is one of the most critical factors in the degradation of perovskite solar cells. Hydration occurs in stages. At moderate humidity, a monohydrate phase forms and the process is partly reversible. With higher humidity or longer exposure, a dihydrate phase develops, followed by irreversible decomposition into lead iodide, hydrogen iodide, and methylamine gas. Under high humidity conditions (~80% RH), surface changes can begin within four hours [42]. The type of electron transport layer strongly influences moisture-related degradation. Titanium dioxide can generate superoxide species under UV light, thereby accelerating interfacial decomposition.

Tin oxide exhibits lower photocatalytic activity and therefore provides better stability in most configurations than TiO_2 [43]. If its surface is not properly controlled, however, NiO_x, which is frequently used in p–i–n devices, can absorb water and create local degradation sites.

When combined, moisture and oxygen are more harmful than when used separately. The partial pressure of oxygen determines their combined effect, which is not well documented in many studies. Moisture and oxygen primarily infiltrate practical modules through edge seals and tiny flaws in the encapsulation layers. Outdoor studies have confirmed that real environmental exposure leads to faster degradation than predicted by single-stressor laboratory tests [39]. This result is a central argument for replacing single-stressor testing with coupled-stressor protocols that better represent field conditions.

3.3. Thermal Stress and Phase Stability

In methylammonium lead iodide, temperatures above approximately 80°C lead to the release of methylamine and hydrogen iodide gases and to irreversible conversion into lead iodide. Formamidinium-based and mixed-cation compositions show better thermal stability, with the active-to-inactive phase transition occurring only above 120-140°C [29]. Thermal cycling creates mechanical stress through mismatches in the coefficients of thermal expansion of adjacent layers. IEC 61215 requires 200 cycles between -40°C and +85°C. Figure 2 illustrates how a strain-compliant encapsulation method maintained 98% efficiency after 1000 hours of damp heat and 95% efficiency after 220 thermal cycles [44]. This result confirms that suitable encapsulation design can substantially reduce thermal damage at the module level.

3.4. Light-Induced Effects and Photo-Activated Defect Chemistry

Perovskites exhibit photoinduced ion redistribution within seconds to hours of light exposure, as well as gradual degradation over thousands of hours of sustained illumination. Under continuous illumination, iodine can oxidise and leave the lattice, creating vacancies that act as recombination centres. In wide-bandgap compositions used in tandem cells, halide segregation under light creates iodide-rich and bromide-rich regions that reduce open-circuit voltage through local bandgap narrowing [14]. Contradictory reports exist regarding reversibility: some studies report partial re-homogenisation during dark storage, while others show cumulative irreversible bandgap narrowing under sustained maximum power point operation. This disparity most likely results from variations in carrier density, strain state, and bromide fraction during illumination. Although strain-relaxed crystal formation, two-dimensional/three-dimensional interface confinement, and compositional engineering are promising mitigation strategies, long-term tandem voltage stability beyond 1000 hours has not yet been well verified at module scale.

3.5. Ion Migration, Hysteresis and Bias Stress

Ion migration is an inherent characteristic of halide perovskites. In methylammonium lead iodide, iodide vacancies migrate with activation energies between 0.3 and 0.6 eV depending on composition. Ion migration has a significant impact on operational stability, as demonstrated by the direct correlation between hysteresis magnitude and T80 lifetime [14]. Ion redistribution enhances recombination and reduces charge transport, as shown by accelerated aging under forward bias in the dark [45]. Although some recovery occurs during dark storage, lasting damage remains. Reversible ion redistribution also drives daily efficiency

fluctuations under outdoor conditions, as confirmed by two years of outdoor monitoring that showed daytime degradation at high temperatures and partial nocturnal recovery [46].

3.6. Mechanical Stress and Module-Level Failure Propagation

The fracture toughness of perovskite films is significantly lower than that of silicon, ranging from 0.1 to 0.3 MPa·m^0.5. In flexible designs, stress can arise from bending, film deposition, thermal-expansion mismatch, and wind loading. Metal halide perovskites (MHPs) are promising candidates for high-performance tandems and next-generation thin-film photovoltaics; however, solution-processed MHP films are vulnerable to residual stress, which can cause unwanted surface wrinkling. One proposed film-formation model suggests that a perovskite top crust forms on a semirigid sol capable of transmitting mechanical forces. Phase transition then generates tension in the MHP crust, while continued shrinkage of the sol induces additional compression and surface wrinkling. When the forces between the sol and the crust are dynamically balanced, wrinkle-free films can be obtained [47]. Electroluminescence images of aged modules frequently show dark lines originating at scribe edges, indicating contact loss due to delamination or cracking in interconnection regions. Non-destructive imaging techniques are therefore needed to detect these mechanically induced failure signals before catastrophic performance loss occurs.

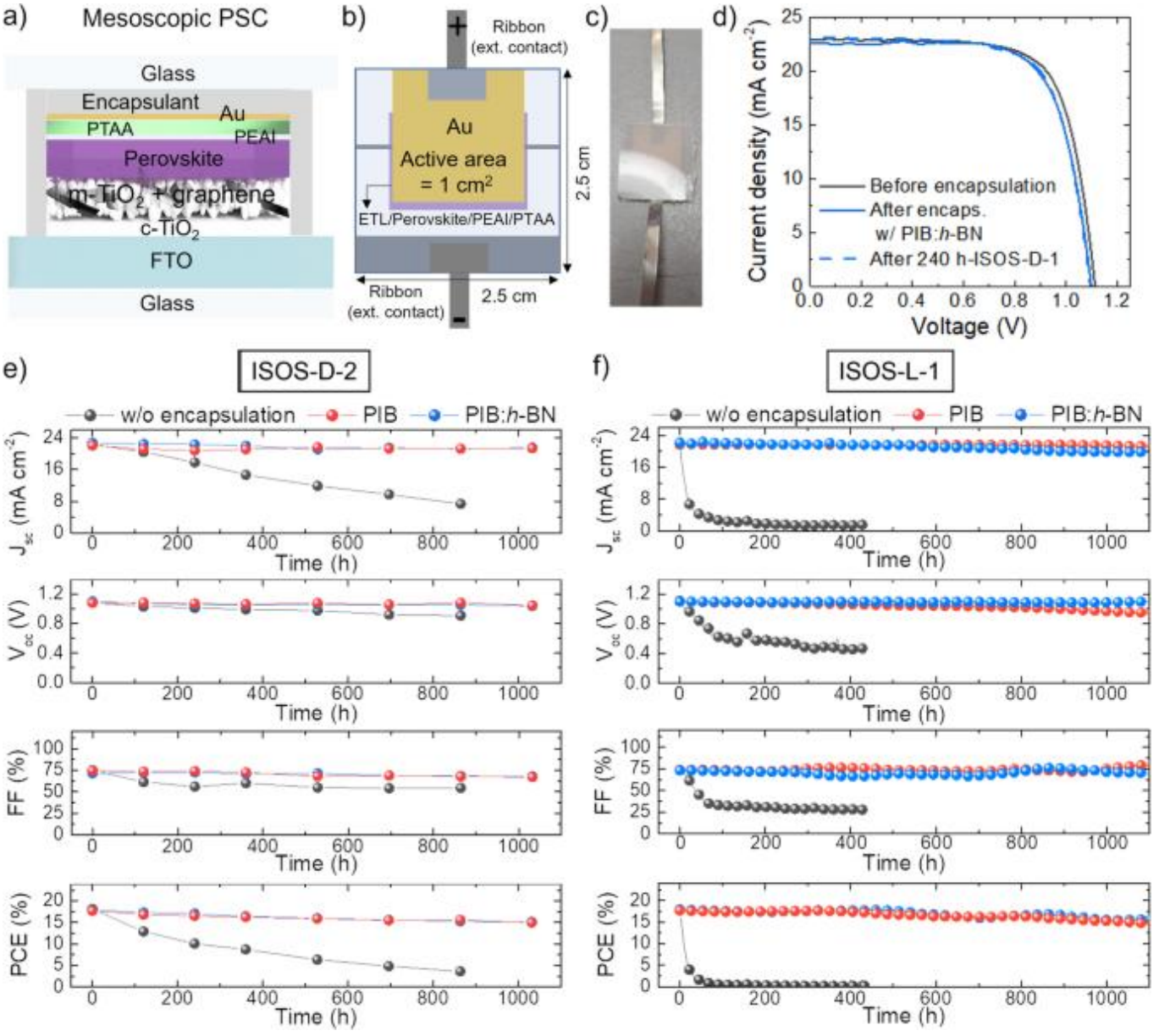

Figure 2. ISOS-D-1/D-2 and ISOS-L-1 stability tests. **(a)** Structure of the mesoscopic n-i-p PSCs. **(b)** Schematic of the cell layout. **(c)** Photograph of a mesoscopic PSC encapsulated with PIB:h-BN. **(d)** JV curves. **(e) (f)** PV parameters of the mesoscopic PSCs [44].

Table 7. Perovskite Module Failure-Mechanism Matrix

Mechanism	Stressor	Origin	Diagnostic	Module Risk	Mitigation	Ref.
Moisture hydrolysis	RH > 60%	Hydrate formation	XRD, EL imaging	Rapid decay, irreversible	Glass-glass encapsulation, PIB seal	[39, 42]
Iodide vacancy migration	Electric field, heat	Low Ea (0.3-0.6 eV)	Impedance spectroscopy	Hysteresis, T80 reduction	Interface blocking, FA-based composition	[14]
Metal contact decomposition	Ion diffusion	Ag-I or Au-I reaction	SIMS depth profile	Series resistance increase, FF drop	Diffusion barrier layer (Cr, Ni)	[29]
Halide segregation	Illumination (wide-bandgap)	Phase separation	Hyperspectral PL	Voc loss, bandgap narrowing	Compositional tuning, 2D/3D interface	[14]
Tin oxidation	Air / O_2 exposure	Sn^{2+} to Sn^{4+}	XPS analysis	Carrier lifetime loss	Reducing additives, strict encapsulation	[9]
Damp heat ingress	85°C / 85% RH	WVTR diffusion	Damp heat test	Delamination, edge degradation	PIB seal, glass lamination	[31]
Interconnect shunt	Laser debris	Thermal damage at P2	EL dark lines	FF drop	Optimized P2 scribing	[20]
Thermal decomposition	T > 80°C (MA-based)	MA volatilization	TGA, mass spec	PbI_2 formation	FA/Cs composition replacement	[29]
UV degradation	UV dose, 280-455 nm	Bond breaking in ETL/HTL	UV aging, EQE	Encapsulant yellowing	UV filter in encapsulant	[48]
Lead leaching	Mechanical damage	Pb solubility in water	Leach test	Regulatory risk	Ion-binding polymer encapsulant	[33]
Mechanical cracking	Thermal cycling	CTE mismatch	EL imaging	Crack propagation from scribes	Strain-compliant interlayers	[32]
Coupled stress synergy	Light + heat + MPP	Nonlinear kinetics	Outdoor monitoring	Underestimated T80	ISOS-O and ISOS-L-2 testing	[39]

3.7. Perovskite Failure Mechanism Matrix

A schematic representation of the Multiphysics Degradation Map under Coupled Stress is presented in Figure 3. Sophisticated diagnostic technologies aid the identification of failure mechanisms. Electroluminescence imaging under forward bias reveals non-uniform current collection, with dark areas indicating shunts or degraded regions. Photoluminescence mapping reveals the distribution of carrier lifetime. By examining peak positions and widths, hyperspectral PL can distinguish phase segregation from general quenching. Impedance spectroscopy uses frequency response to differentiate ionic and electronic processes. SIMS and XPS depth profiling track iodide, lead, dopants, and metal atoms across layers. These methods reveal chemical events and diffusion pathways that are not visible to optical inspection. The predominant degradation mechanisms documented in current research are summarised in Table 7, which links module-level risks, physicochemical origins, diagnostic signs, triggering stressors, and the most relevant mitigation techniques. The objective is to provide a structured failure-mechanism matrix that clearly identifies which pathways are primarily cell-level phenomena and which critically affect module bankability, as discussed in Section 3.1.

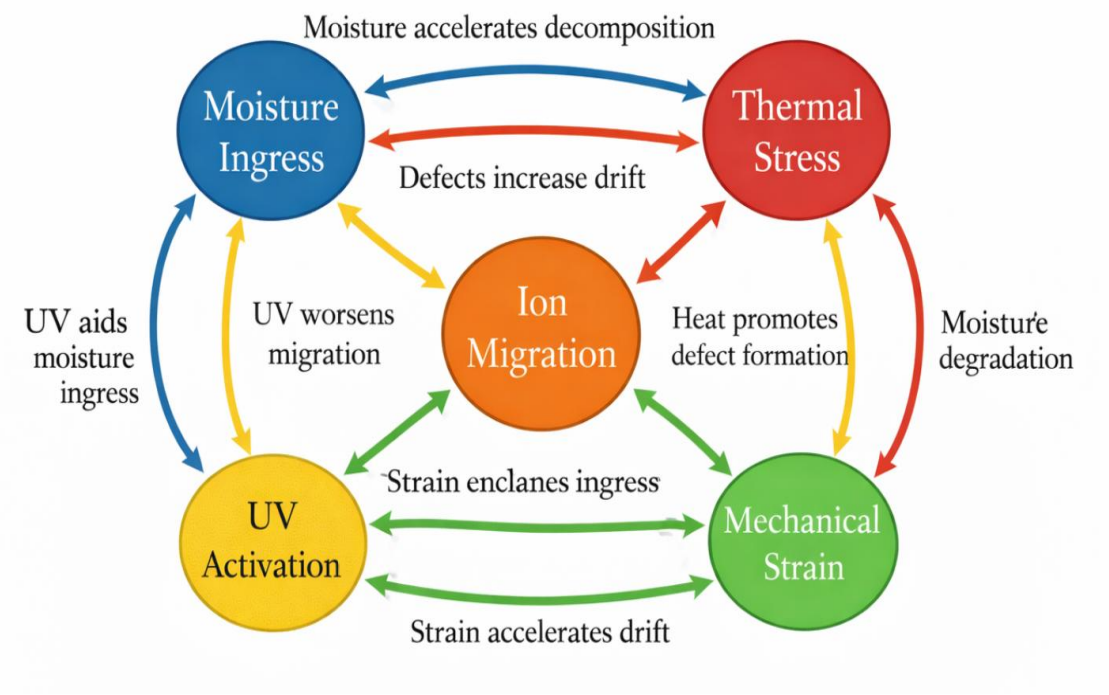

Figure 3. Multiphysics Degradation Map under Coupled Stress

4. Charge Transport Interfaces and Contact Stability

Grain boundaries and surface regions in polycrystalline perovskite films contain many more defects than the bulk material. Trap density at surfaces can be nearly two orders of magnitude higher than inside the grains. Such defects reduce carrier lifetime and limit efficiency. Combined bulk and surface passivation strategies have helped increase single-junction device performance from approximately 22% to nearly 26% [49-51]. Post-treatment with benzylammonium iodide applied by slot-die coating improved carrier lifetime and spatial uniformity in large-area films, confirming that scalable passivation methods can maintain high performance at module scale [50]. Two-dimensional perovskite capping layers formed by large organic cations such as phenethylammonium or butylammonium provide an effective strategy for surface passivation. These layers reduce surface traps, block ion movement, and increase moisture resistance. Devices based on this two-dimensional/three-dimensional structure achieved efficiencies above 23% and maintained 99% of their initial performance for more than 2000 hours under ISOS-L-1 conditions [29]. Bulk passivation through additive engineering targets defects inside the film. A thiourea-based additive formed a self-assembled layer at the buried interface, producing a certified cell efficiency of 23.75%. A blade-coated module with a 60.84 cm² aperture area reached 20.18% efficiency and retained more than 90% of its performance for over 1000 hours under maximum power point operation, as shown in Figure 4 [51]. This study demonstrated that efficiency and stability can improve together at module scale.

Tin oxide has become the preferred electron transport layer in high-efficiency n-i-p devices because of its suitable conduction-band alignment, efficient electron extraction, and better UV stability compared with titanium dioxide [43]. In p-i-n devices, fullerene materials such as C60 serve as electron transport layers. Self-assembled monolayer hole contacts, such as carbazole-based phosphonic acid materials like 4PACz and MeO-4PACz, provide a thin and uniform alternative to Spiro-OMeTAD. These layers reduce interface recombination, enable open-circuit voltage close to the radiative limit, and are compatible with scalable fabrication [17]. Gold and silver back electrodes used in laboratory devices are susceptible to iodide diffusion and the formation of low-conductivity halide compounds. Barrier layers between transport layers and metal contacts slow halide diffusion and improve long-term stability [41]. Carbon electrodes provide a corrosion-resistant alternative and show strong stability, although efficiency may be slightly reduced because of limited hole-extraction kinetics.

5. Scalable Manufacturing Pathways and Process Windows

The shift from laboratory spin coating to industrial deposition methods is a major challenge for perovskite commercialisation. Spin coating wastes nearly 90% of precursor solution and does not support continuous production on substrates larger than approximately 10 cm by 10 cm. Scalable techniques including blade coating, slot-die coating, spray coating, inkjet printing, and vapour-based processes have therefore attracted significant attention [20, 52].

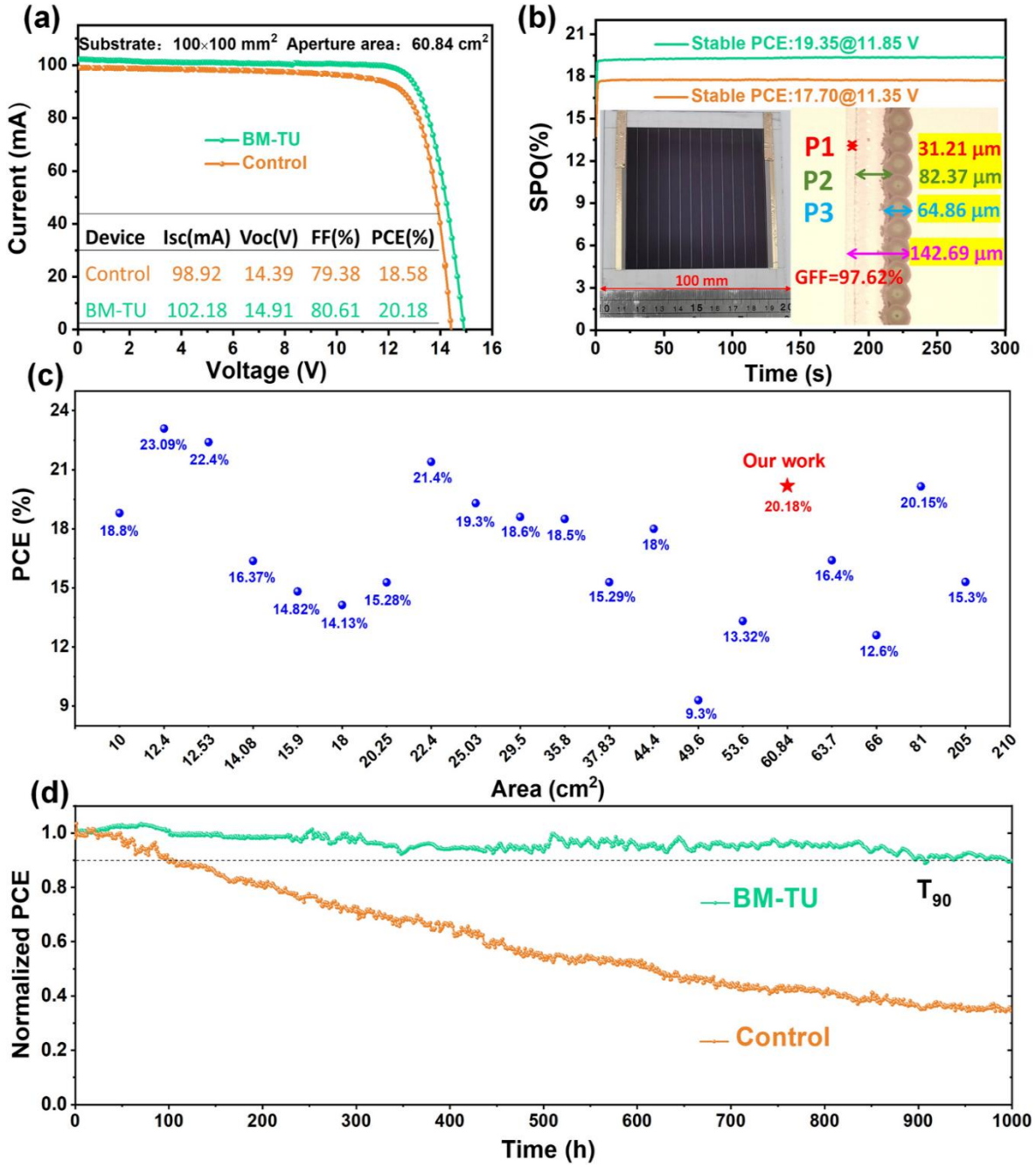

Figure 4. (a) J–V characteristics of the perovskite solar module with an aperture area of 60.84 cm². **(b)** Steady-state PCE of the perovskite solar module (Inset 1 is a photograph of the fabricated perovskite solar module; inset 2 shows microscope images of the P1, P2, and P3 scribe lines in the dead area of the PSMs). **(c)** Summary of PCE for solar modules based on blade coating in recent years. **(d)** MPPT performance of the perovskite solar module [51].

Blade coating offers material utilisation above 90% and supports substrates up to at least 15 by 15 centimetres. A blade-coated NiOx p-i-n module with 110 cm² active area achieved 12.6% efficiency and retained 84% of its performance after 1000 hours at 85°C under ISOS-T-1 conditions [52]. Slot-die coating delivers ink through a narrow slot onto a moving substrate, allowing precise wet film thickness control and supporting roll-to-roll production [53]. Common laboratory solvents such as dimethylformamide and dimethyl sulfoxide are classified as reproductive toxins under regulatory guidelines. Safer solvent systems are necessary for large-scale production. Recent study indicates that green solvent systems can achieve comparable efficiencies while improving reproducibility [24]. Gas quenching directs dry nitrogen or air over the wet film to control nucleation in a manner compatible with continuous processing. With optimised flow and temperature, gas quenching can produce uniform films over areas up to 60 cm². This approach was demonstrated using a thiourea-based additive engineering strategy, achieving a blade-coated module efficiency of 20.18% [51].

Figure 5 shows an R2R-processed roll with the constituent layers of PSCs after each layer was manually removed.

Ambient-air processing is necessary for economic viability at gigawatt scale. A slot-die deposition study using a pyrrodiazole additive and controlled lead iodide immobilisation produced 10 cm × 10 cm modules with certified 20.3% efficiency, retaining 94% of their efficiency after 1000 hours under illumination at 65% humidity [27]. Through continuous monitoring of key film properties, in-line metrology enables real-time process control during deposition. Wet-film thickness and solvent-evaporation dynamics can be monitored by optical reflectometry, which provides rapid feedback on coating homogeneity. This is further supported by in-line photoluminescence imaging, which allows early detection of non-uniformities by mapping carrier lifetime across the substrate immediately after film formation. In addition, defective films can be automatically identified by machine-vision systems trained on validated reference datasets before further processing. This strategy is supported by a two-year outdoor study that demonstrated the value of data-driven process optimisation by estimating power production from monitored operational data using a regression-based predictive model [46].

6. Module Design, Interconnection, and Encapsulation

Monolithic perovskite modules use a P1-P2-P3 laser scribing sequence to define and connect subcells.

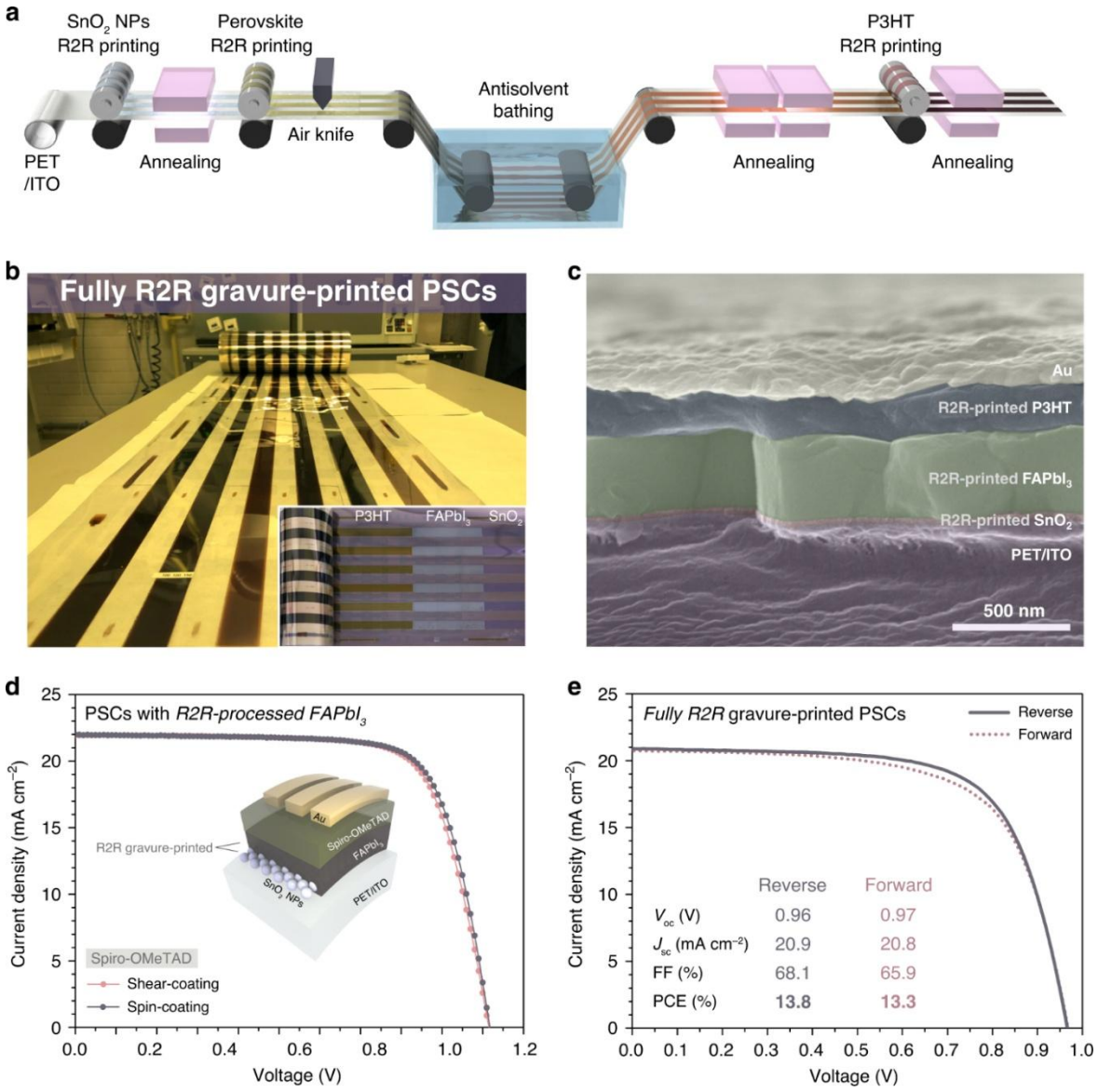

Figure 5. (a) Diagram showing R2R processing for the fabrication of flexible PSCs. **(b)** Photograph of fully R2R-processed PSCs. (Inset) Image of an R2R-processed roll showing the constituent layers of PSCs after each layer was manually removed. **(c)** Cross-sectional SEM image of fully R2R-printed PSCs, with each layer shown in a different colour. **(d)** J–V curves of a champion device made from R2R-processed SnO_2/perovskite and Spiro-OMeTAD (shear-coating: purple; spin-coating: indigo). **(e)** J–V curves of fully R2R gravure-printed PSCs. FAPbI3 denotes (FAPbI3)0.95(MAPbBr3)0.05 [55].

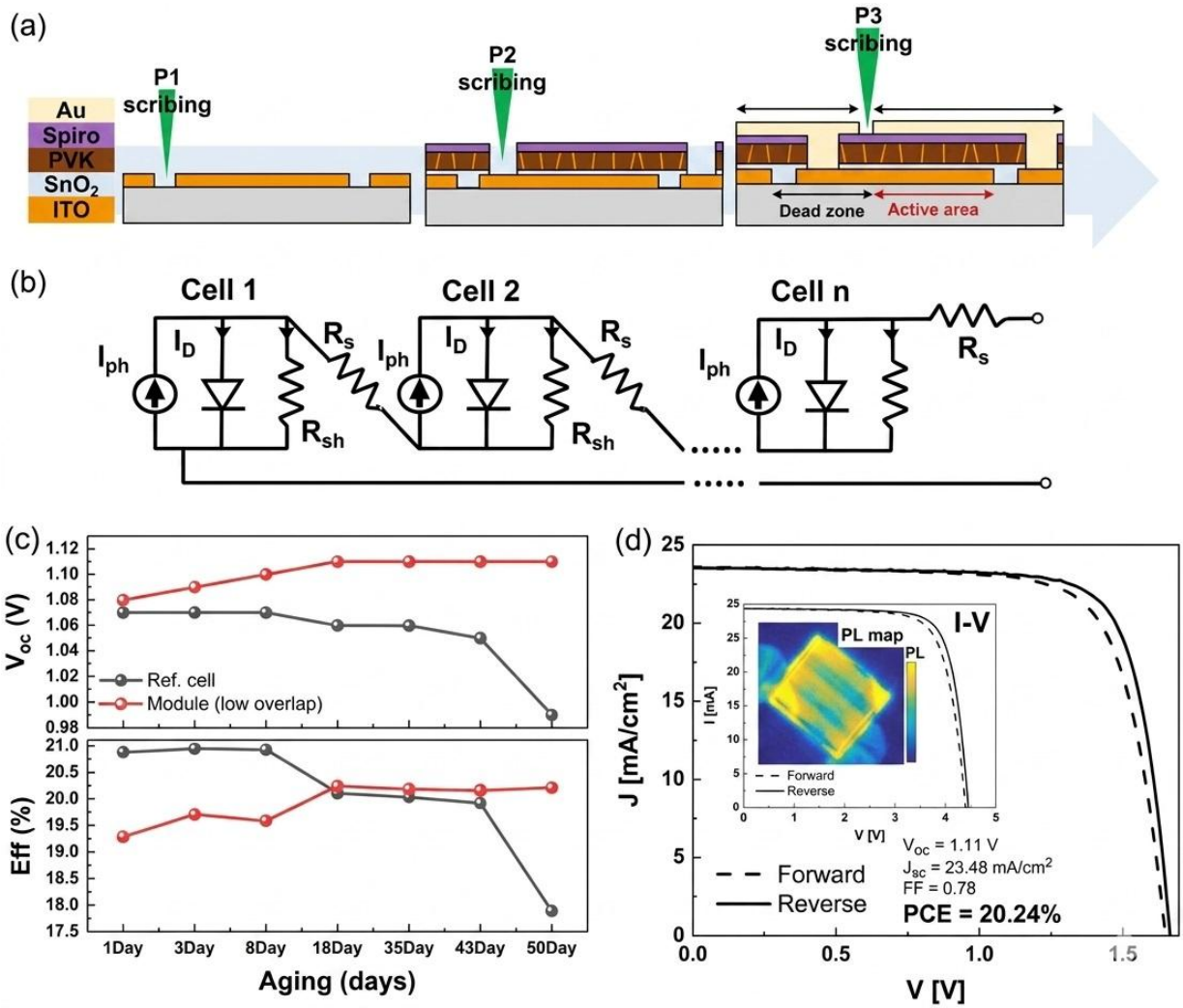

Figure 6. (a) Fabrication process of a perovskite solar module with all-laser scribing (the scribing steps are composed of P1–P2–P3). **(b)** Equivalent circuit of a monolithically interconnected module (Iph: photocurrent, ID: diode current, Rs: series resistance, Rsh: shunt resistance). **(c)** Comparison of efficiency and VOC in the reference cell and module under low-power and low-laser-overlap conditions over time. **(d)** J–V curve of the best perovskite module using an optimised P3-scribing condition. The module efficiency is 20.24% (after 18 days of aging). The active area of the module is 5 cm², and the inset shows a photograph of the perovskite module [55].

Figure 6 shows the fabrication process of a perovskite solar module with all-laser scribing (P1-P2-P3) [55]. This process determines dead-area fraction, shunt resistance at scribe edges, and possible damage to underlying layers. Laboratory-optimised scribing typically creates total dead widths between 300 and 600 micrometres per interconnect. For cell pitches of 5-10 millimetres, this produces a dead-area fraction of approximately 5-10% [56]. Silicon thin-film modules have reduced dead area below 4% after many years of optimisation, indicating that further improvement is possible in perovskite interconnect design [57]. Module series resistance arises from transparent electrode sheet resistance, contact resistance at P2 interconnects, and metal back contacts. For a module with an 8 millimetre cell pitch, 12 ohms per square indium tin oxide, and 20 mA cm^{-2} current density, the electrode resistance alone can reduce fill factor by approximately 2-3%. The optimal cell width for standard indium tin oxide lies between 5 and 10 millimetres [19].

Encapsulation is critical for long-term stability. Perovskite devices require water-vapour transmission rates close to 10^{-4} to 10^{-5} grams per square metre per day, much lower than the values acceptable for silicon modules [58, 59]. Glass-glass lamination designs meet this requirement. Among polymer materials, polyolefin elastomers and polyisobutylene-based encapsulants show good performance. A comparison between commercial glass-glass lamination and laboratory glue sealing showed that commercially laminated devices retained more than 95% efficiency after 1566 hours at 85°C and 85% relative humidity and maintained performance for more than 10 months during rooftop outdoor exposure [58]. A low-temperature encapsulation method using a viscous adhesive laminated below 80°C achieved 98% efficiency retention after 1000 hours of damp heat and 95% retention after 220 thermal cycles [44].

Conventional ethylene-vinyl acetate encapsulant is not suitable for many perovskite systems because it releases acetic acid during processing. Ionomer materials have high stiffness and can promote delamination during thermal cycling. Edge seals based on polyisobutylene butyl rubber control moisture ingress at the module perimeter. Perovskite modules contain approximately 0.5-2 grams of lead per square metre. Rainwater can readily dissolve methylammonium lead iodide. Impact-testing studies show that unprotected perovskite modules can release lead concentrations that exceed legal leachate limits when the modules are broken. Leached lead concentrations are reduced by more than 90% in encapsulation systems that include ion-binding polymers based on phosphonate, carboxylate, or amino groups [59]. By keeping lead release within legal limits, shellac-based encapsulation has enabled modules to pass mechanical and UV tests under IEC 61215 standards [59]. The development of standardised impact-leach testing procedures for perovskite modules is still ongoing.

7. Reliability, Standardisation, and Qualification-Style Testing

7.1. Why Stability Claims Are Often Not Comparable

According to the stability literature, T80 values for perovskite solar cells range from less than 100 hours to more than 10,000 hours. Because testing conditions, measurement techniques, and encapsulation strategies differ substantially across studies, these figures cannot be directly compared. The primary causes of inconsistency were outlined in a consensus statement on ISOS protocols [60]. These include whether efficiency was measured at maximum power point or from current-voltage scans, the scan rate, the encapsulation technique, the test atmosphere, temperature, light intensity, and spectrum, and whether T80 was determined directly or extrapolated from partial data. Because performance, stability, qualification, and techno-economic studies represent fundamentally different evidence types, they are presented separately in this review.

Particular attention should be given to the distinction between the ISOS-L-1 and ISOS-L-2 protocols. ISOS-L-1 uses continuous one-sun illumination under open-circuit conditions. Under otherwise comparable lighting conditions, ISOS-L-2 employs maximum power point tracking. Because the internal electric field differs substantially between these two conditions, ion redistribution and degradation rate are also affected. Compared with ISOS-L-2 measurements on the same devices, T80 values obtained under ISOS-L-1 consistently overestimate operational lifetime. Only ISOS-L-2 data have actuarial significance for bankable warranty claims because they reflect the conditions under which a module in a solar power plant actually operates and generates revenue.

7.2. Recommended Reporting Checklist

For meaningful inter-study comparisons and informed bankability evaluations, clear reporting requirements are essential. The ISOS consensus guidelines [60] and the IEC qualification framework [6] both specify the information that must be reported to ensure the validity of performance claims.

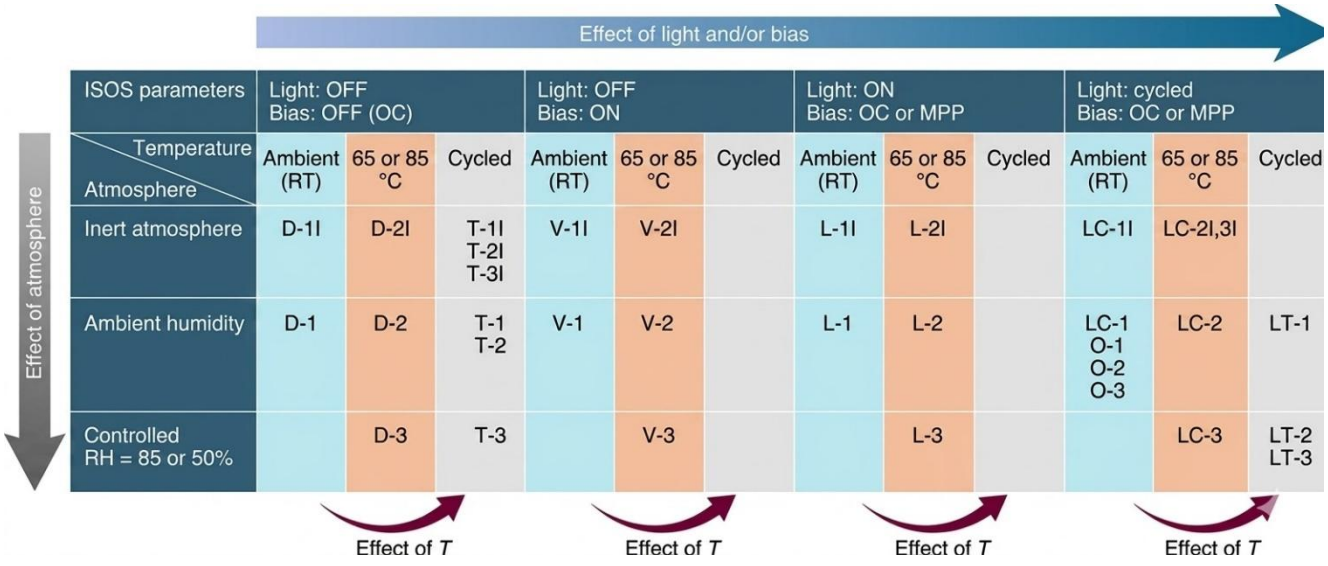

Figure 7. Rows correspond to different atmospheres, columns correspond to different combinations of light and electrical bias, and sub-columns depict different temperature regimes. Arrows alongside the table guide the eye for comparing protocols to identify the effects of atmosphere, temperature, light or electrical bias [60].

These include the number of devices tested, the effective aperture area of the module together with any inactive (dead) areas, and the corresponding mean values and standard deviations for key metrics such as initial efficiency and stability indicators like T80 or T90. It is also essential to state whether the reported lifetime numbers were obtained by direct measurement or by extrapolation. The analysis should be supported by imaging data, such as electroluminescence or photoluminescence maps recorded before and after aging. If a study does not include these basic elements, its findings should be treated only as preliminary (Category A) evidence and should not be used for detailed or quantitative bankability assessments.

7.3. Accelerated Stress Tests: Light/Heat/Humidity/Bias and Coupled Stressors

Thermal cycling, outdoor testing, light exposure, and dark storage are all covered by the ISOS protocol family. However, these protocols do not fully address the sequential qualification logic outlined in IEC 61215, which considers module-level stresses such as encapsulation failure, framing stress, and interconnection degradation. IEC 61215 requires only 15 kWh/m² of UV exposure, which is substantially lower than the cumulative UV dose expected over 25 years of outdoor operation. The standard was developed for silicon modules and does not account for ionic migration effects unique to perovskites [6]. A long-term study of UV effects showed that wavelengths between 280 and 455 nm contribute substantially to degradation; however, isolating UV effects from other stressors during outdoor exposure remains challenging [61]. A two-year outdoor study of minimodules under ISOS-O conditions observed degradation during sunlight and partial overnight recovery, with accumulated degradation showing a linear relationship with total irradiance dose [46]. These results confirm that single-stressor tests systematically underestimate field degradation.

7.4. Linking Accelerated Testing to Field Performance

One major outstanding issue is translating accelerated-test results into actual outdoor lifetime. Some sources have claimed a 20-year lifespan by extrapolating from wet-heat tests lasting several thousand hours. Such extrapolation has been criticised because degradation mechanisms under accelerated conditions may differ from those operating outdoors [39]. Although the number of studies on the outdoor stability of PSCs has increased, much more work is needed to establish acceleration factors for different aging protocols and to link accelerated-test results with real-world performance. It is therefore necessary to examine the relationship between outdoor and accelerated aging results across different solar-cell types. To build robust degradation models and determine reliable acceleration factors, more data must be gathered from extensive outdoor testing of different perovskite devices under standardised conditions. More credible evidence comes from studies that directly compare accelerated IEC damp-heat results with the outdoor performance of the same devices [62]. This practice should become standard in publications intended to inform bankability.

7.5. Toward PV Qualification Logic

Regulatory backing and technological consensus are needed to develop a formal qualification standard for perovskite modules. A tiered qualification approach offers a practical and useful path forward. To meet the requirements for pre-bankable demonstration status, Tier 1 modules must exhibit light and UV stability together with effective moisture protection under ISOS conditions. Tier 2 modules must individually satisfy IEC 61215 requirements for mechanical load, damp heat, and thermal cycling. Tier 3 modules must pass the Tier 2 tests sequentially and demonstrate at least 12 to 24 months of outdoor monitoring in at least two representative climate zones, with annual degradation below 1% supported by statistical confidence intervals. Completion of Tier 3 is necessary for bankable deployment. Financial bankability also requires warranty structures to be defined in actuarially priceable terms. Standard photovoltaic warranties typically guarantee less than 2% first-year efficiency loss and less than 0.5-0.8% annual degradation thereafter. Translating perovskite stability metrics into such warranty structures requires statistically validated outdoor degradation distributions from multiple modules across multiple climate zones, not single-device T80 claims. Without quantified variance in degradation rate across a production batch, actuarial risk pricing for perovskite warranties remains infeasible. The bankability evidence package defined in Section 9.2 specifies the minimum data requirements needed to support such pricing.

8. Techno-Economic and Sustainability Considerations

8.1. Cost Drivers, Yield Sensitivity and Bankable Economics

The economic potential of perovskite photovoltaics rests on two foundations. First, higher efficiency reduces area-related balance-of-system costs. Second, low-temperature and solution-based processing can reduce manufacturing cost relative to silicon. A bottom-up cost analysis showed that single-junction perovskite modules can compete with silicon if module efficiency reaches 25% and production yield exceeds 95% [63]. A sensitivity analysis indicates that increasing the annual degradation rate from 0.5% to 1.5% raises levelised cost of electricity by approximately

8-15% under constant efficiency assumptions. Similarly, reducing manufacturing yield from 95% to 85% increases module cost per watt by 10-18% [63]. These are not arbitrary engineering targets. They are economic inflection points that define the boundary between competitive and uncompetitive products in utility-scale solar markets. A techno-economic model for European markets indicated that cost competitiveness requires either efficiency above 24% with a 20-year lifetime or efficiency above 20% with a 30-year lifetime [12]. For perovskite-silicon tandems, levelised cost of electricity can decrease by 10-20% compared to silicon modules under a scenario of module efficiency above 30% and manufacturing cost only slightly higher than silicon [64].

8.2. Environmental and Regulatory Considerations

Environmental performance and regulatory compliance are not peripheral concerns for perovskite modules; they are integral components of the bankability framework. A module that achieves excellent certified efficiency and passes IEC qualification tests is still not bankable in regulated markets if its regulatory acceptance remains unresolved. This review therefore treats environmental and regulatory readiness as a fifth dimension of bankability assessment, alongside efficiency, stability, manufacturing yield, and qualification compliance. Life-cycle assessments show that perovskite modules have competitive energy payback times and greenhouse gas emissions compared with other thin-film technologies [65]. However, lead containment during operation and at end-of-life remains a critical regulatory requirement. Lead use in photovoltaics is currently exempt from EU regulations under the Restriction of Hazardous Substances framework, but this exemption is reviewed regularly. An unfavourable future review could effectively prohibit the sale of perovskite modules in European markets, posing a significant financial risk to investors and developers. Perovskite manufacturers operating in or targeting regulated markets must therefore remain compliant with evolving regulations.

Lead containment in the event of module breakage is a technical requirement that must be incorporated into encapsulation design rather than treated as a secondary concern. Impact-testing studies show that, under simulated breakage conditions, unprotected modules can release lead concentrations that exceed regulatory leachate standards. Encapsulation systems that use ion-binding polymers can reduce leached lead concentrations by more than 90% [59]. The bankability evidence package outlined in Section 9.2 should include this technical solution as a minimum requirement. The bill of materials for bankable modules should also include predefined end-of-life recycling routes. A proven recycling strategy for glass, indium tin oxide substrates, and other recoverable materials can reduce both the life-cycle cost and the regulatory risk of perovskite modules [65]. In markets with extended producer-responsibility laws, developers may face difficulties in obtaining construction licences and project insurance if they cannot present an approved end-of-life management plan.

8.3. Manufacturing Readiness Levels and Commercialisation Pathways

According to manufacturing-readiness assessments, perovskite photovoltaic technology currently lies between Manufacturing Readiness Levels 4 and 5. Large-scale yield control, consistent throughput, and supply-chain integration have not yet been demonstrated, but the technology has been validated at relevant laboratory scale and initial pilot-line production has begun. It is important to distinguish among four stages of manufacturing maturity, which are often conflated in peer-reviewed journals and the commercial press. The first stage is pilot-line existence, meaning that a facility has been built and preliminary modules have been produced. This demonstrates technical capability and ambition, but it provides no information about production control. The second stage is stable throughput, which refers to the ongoing production of modules at a defined rate with acceptable equipment uptime. This indicates competent process engineering, but it does not prove product quality. The third stage is yield-controlled production, defined as statistically monitored batch yield consistently above 95% with a coefficient of variation below 5% over several months of production runs. This is the minimum requirement for credible bankable cost models. The fourth stage is independent field validation, which requires modules from the same production line to be independently verified, deployed in the field, and monitored for at least 12 months using publicly accessible performance data. Only at this level does an evidence base exist for actuarial warranty pricing.

At least one gigawatt-scale manufacturing line has been announced, and other companies have launched pilot lines for single-junction modules ranging from 10 to 150 megawatts per year [10]. These announcements correspond to Level 1 manufacturing maturity. Progress toward Level 2 is indicated by a perovskite-silicon tandem installation demonstrating module-scale products operating in real outdoor environments [66]. At present, there is no evidence that perovskite modules have reached Level 3 or Level 4 maturity. Before IEC standardisation, crystalline silicon experienced multiple reliability failures and took around 20 years to progress from Level 1 to Level 4. Compared with the historical trajectory of silicon, perovskites have advanced more quickly in efficiency but remain at an earlier stage of reliability maturity.

9. Roadmap: What Will Move the Needle in the Next 24 Months

9.1. Top Technical Priorities

The gap analysis performed in this review identifies specific technical priorities for the next two years. In the stability domain, single-stressor testing must give way to coupled-stressor conditions. Under ISOS-L-1, many devices already achieve T80 values above 1000 hours. The next essential milestone is a T80 above 1000 hours under simultaneous light exposure, a temperature of about 65°C, and maximum power point operation. This threshold represents about 25% of the 4000 hours often used as a proxy for a 20-year lifetime under accelerated conditions. It is therefore a necessary, though not sufficient, milestone for bankable lifetime claims. A more credible benchmark would be a T80 above 5000 hours under ISOS-L-2 at 65°C. Long-term outdoor data from at least two different climate zones must also be collected and made publicly available to build the statistical basis for actuarial warranty pricing.

Module efficiencies greater than 20% must be demonstrated through scalable manufacturing using fully scalable processes on substrates larger than 200 cm². A threshold of 20% on substrates above 200 cm² represents the minimum performance level at which perovskite modules can economically compete with high-end crystalline silicon products in utility-scale applications. Process variation between batches should remain below a 5% coefficient of variation. Meeting this target would demonstrate that performance is not limited to isolated laboratory samples and would move the field from Category A to Category B reproducibility evidence. In module design, reducing dead-area fraction below 5% and achieving geometric fill factors above 95% are realistic engineering goals given recent progress in scribing optimisation.

In encapsulation, glass-glass structures must pass IEC 61215 damp-heat and thermal-cycling tests sequentially rather than individually. For tandem modules, certified efficiency above 30% on aperture areas greater than 100 cm² is the next key target. All-perovskite tandems remain particularly challenging because of tin oxidation in the narrow-bandgap subcell [9]. For perovskite-silicon tandems, uniform crystallisation and effective buried-interface passivation on textured silicon substrates have enabled certified 24.5% efficiency on a 20.25 cm² module [18], providing a benchmark from which 30% module efficiency on 100 cm² can be framed as the next major milestone.

9.2. Minimum Data Package for Bankable Claims

The following evidence package represents the minimum dataset that an independent engineer, insurer, or project financier would require before accepting a warranty-backed commercial claim for a perovskite module. These requirements are derived from the financial-risk assessment standards used in photovoltaic projects by major independent engineering firms and from the qualification framework discussed in Section 7. The package has five mandatory components. The first component is certified module efficiency. A certified aperture efficiency must be obtained from an accredited third-party laboratory on modules with an aperture area greater than 100 cm². The certification must include current-voltage curves, stabilised power output under maximum power point tracking for at least 5 minutes, and a clearly stated uncertainty analysis. The aperture-area basis specified in Table 1 must be used for the measurements. This criterion is not satisfied by measurements made on smaller active areas or under non-standard illumination conditions.

The second component is statistical manufacturing data. Performance data must be provided for at least 50 modules produced over three consecutive production cycles. The dataset must include power conversion efficiency, open-circuit voltage, short-circuit current density, and fill factor, together with the corresponding mean, standard deviation, and coefficient of variation. For power conversion efficiency, the coefficient of variation must be below 5% in every run. This is the minimum amount of data needed to price actuarial warranty risk and validate a cost model. The third component is sequential IEC qualification evidence. Modules must pass IEC 61215-related tests in the following order: humidity-freeze testing, 200 thermal cycles between -40°C and +85°C, and damp heat for 1000 hours at 85°C and 85% relative humidity. Outdoor studies indicate that degradation rates can differ significantly from single-stressor laboratory tests [39]. Electroluminescence imaging must document device condition before, during, and after each test. Throughout the sequence, efficiency retention must remain above 95% of the initial value.

The fourth component is outdoor-monitoring data. Performance monitoring must cover at least 12 months in two distinct climate zones, including one temperate location and one high-irradiance location. To calculate performance ratio and annual degradation rate, monitoring must use maximum power point tracking together with continuous irradiance measurement. Based on the distribution of degradation rates across the monitored module population, the annual degradation rate must be below 1%, with a stated 95% confidence interval. A single-module result is insufficient for this component. The fifth component is regulatory and end-of-life documentation. Lead content per square metre must be specified in the bill of materials. An authorised end-of-life management plan that complies with local laws in the intended market must also be provided. When ion-binding encapsulants are used to address lead containment, the evidence package must include

third-party leach-test results demonstrating compliance with relevant regulatory criteria.

9.3. Perovskite Module Readiness Index (PMRI)

This review proposes a Perovskite Module Readiness Index to quantitatively combine manufacturability, durability, efficiency, and certification progress within a single evaluation framework. The index comprises four normalised parameters: the ratio of certified aperture module efficiency to a 30% benchmark, the ratio of T80 under maximum power point operation to 10,000 hours, the ratio of statistically validated batch manufacturing yield to 95%, and the fraction of required sequential IEC qualification tests that have been successfully completed. The formula is expressed as:

$$PMRI = (CAM_{module} / 30\%) \times (T80_{MPP} / 10{,}000\ h) \times (Yield / 95\%) \times (IEC_{pass\_fraction}) \quad (2)$$

The multiplicative structure of the index is justified by the cross-domain dependency analysis in Section 1.3. A deficiency in any single parameter proportionally reduces overall readiness because the domains are not independently optimisable. A module with excellent efficiency but poor qualification compliance cannot obtain bankable warranty coverage. A module with excellent stability but poor yield cannot achieve the cost targets required for utility-scale project approval. The multiplicative form ensures that the index captures this interdependence and appropriately penalises single-domain failures. The normalisation targets are calibrated against the bankability thresholds developed in Section 9.2. The 30% efficiency standard aligns with next-generation tandem-module targets that would provide clear levelised cost-of-electricity advantages over high-end silicon products. A T80 of 10,000 hours under ISOS-L-2 conditions provides a minimally credible extrapolation basis for a 20-year outdoor lifetime warranty. The 95% yield level is the economic turning point identified in Section 8.1, below which module cost per watt rises by more than 10% compared with the bankable scenario. Sequential qualification compliance is normalised by the IEC pass fraction against the complete test sequence defined in Section 9.2.

The following illustrative values are obtained by applying the PMRI to representative published module examples. The 216 cm² lead-halide perovskite submodule reported in reference [4] has a certified aperture efficiency of 20.6%. However, because the same source does not provide matched ISOS-L-2 operational-stability data, manufacturing-yield statistics, or sequential IEC qualification evidence, a reliable PMRI cannot be calculated from that record alone. The 60.84 cm² blade-coated module in reference [28], with 20.18% efficiency, a T90 above 1000 hours under ISOS-L-2, and similarly incomplete qualification evidence, yields only a partial readiness picture rather than a full PMRI. A pre-bankable threshold of PMRI greater than or equal to 0.7 corresponds to conditions in which efficiency exceeds 20%, T80 under ISOS-L-2 exceeds 7000 hours, yield exceeds 90%, and at least 70% of the sequential IEC test sequence has been completed.

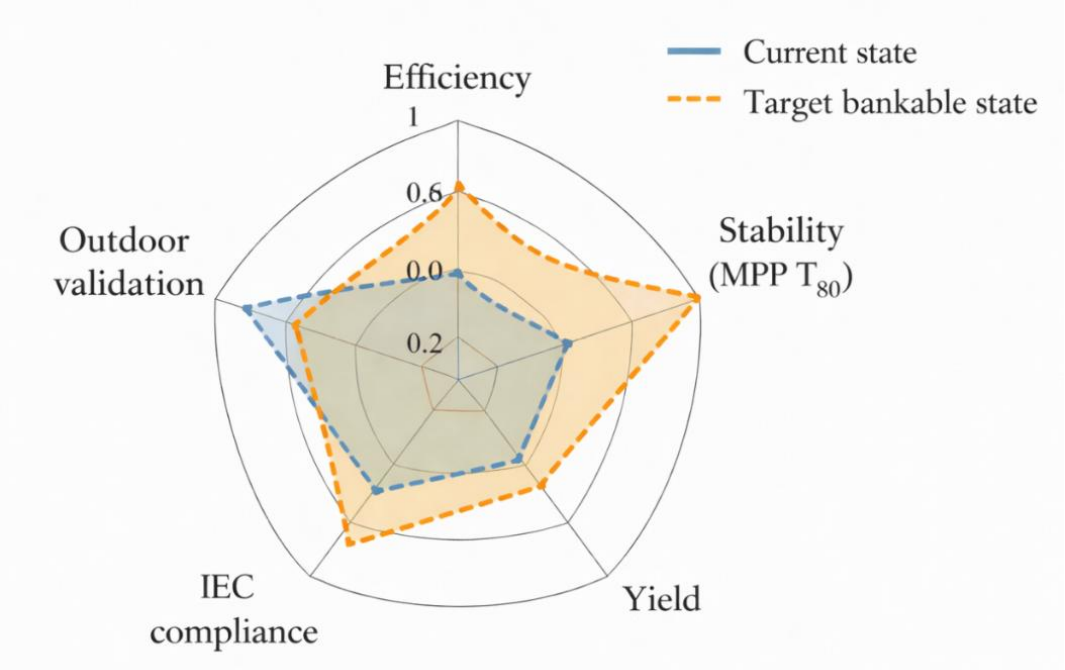

Figure 8. Perovskite Module Readiness Index

No published module currently meets this threshold. A bankable threshold of PMRI equal to or greater than 1.0 corresponds to full satisfaction of the minimum evidence package defined in Section 9.2. Figure 8 compares the current and target bankable readiness index for perovskite modules.

9.4. Open Challenges and Research Opportunities

Several research challenges remain open. The most important is the development of predictive lifetime models that link ion-migration parameters, including activation energy, defect density, and diffusion coefficients, to quantitative T80 predictions under outdoor conditions. Ion migration has been identified as a dominant cell-level degradation factor [14], but module-level lifetime modelling still lacks quantitative validation against outdoor field data. A second challenge is achieving Category C reproducibility, as defined in Section 2.3, at pilot-scale manufacturing volumes. A third challenge is the development of lead-free perovskite compositions based on tin, bismuth, or antimony that can match the efficiency of lead-based systems without suffering severe instability caused by defect formation or tin oxidation [60]. Whether perovskite photovoltaics can meet the reliability threshold needed for widespread utility-scale deployment will depend on progress in all three areas.

10. Conclusion

The efficiency gains achieved in perovskite photovoltaics represent one of the most rapid advances in the history of semiconductor solar technology. Certified single-junction perovskite efficiency has surpassed 26.95%, while perovskite-silicon tandems have reached efficiencies above 34.6%. Yet the central issue highlighted in this review is not efficiency itself; rather, it is the absence of validated, statistically reproducible, and financially priceable evidence needed to support a commercial module warranty claim. The gap between small-area cell measurements and large-area module performance, the inconsistency in degradation reports, and the lack of Category C reproducibility data do not merely represent short-term technical obstacles. They define the distance between the current state of the art in perovskite photovoltaics and the requirements of photovoltaic project finance. This review makes three key contributions. First, it presents a four-domain translation framework with explicit cross-domain analytical dependencies, showing how the efficiency, degradation, engineering, and financial domains interact in ways that cannot be resolved by optimising a single domain in isolation. Second, it separates the evidence into four distinct classes: certified performance, operational stability, qualification-relevant module tests, and techno-economic studies. This avoids misleading comparisons between fundamentally different evidence types. Finally, it proposes a Perovskite Module Readiness Index that translates the four-domain framework into a measurable composite metric calibrated against the bankability criteria defined in the minimum evidence package. It also defines the five-component minimum evidence package that an independent engineer, insurer, or project financier would require before accepting a warranty-backed commercial claim.

For perovskite photovoltaics to reach true commercial readiness, several key performance and reliability targets must be achieved simultaneously. First, devices should demonstrate a certified aperture efficiency above 20% on substrates larger than 200 cm² using processes that can be scaled for industrial production. In addition, operational stability must be demonstrated with a T80 lifetime exceeding 5000 hours under ISOS-L-2 conditions, where devices are exposed to combined light, heat, and maximum power point stress. From a manufacturing perspective, consistency is equally important, with batch yields expected to exceed 95% and variation kept below 5% across repeated production cycles. The technology must also pass standard reliability tests, including the IEC 61215 sequence for damp heat, thermal cycling, and humidity freeze, while maintaining more than 95% of its initial efficiency. Finally, real-world performance should be validated through at least one year of outdoor testing in two different climate zones, with annual degradation below 1% and clearly reported statistical confidence. Together, these benchmarks define a practical pathway toward bankable commercialisation. Recent literature shows progress toward these five milestones, although no published result yet satisfies all of them simultaneously. The path forward for the photovoltaic community should therefore be guided by these five conditions rather than by overly optimistic forecasts that cannot yet be substantiated.

References

[1] X. Fan, Advanced Progress in Metal Halide Perovskite Solar Cells: A Review. Materials Today Sustainability, 24, (2023) 100603. https://doi.org/10.1016/j.mtsust.2023.100603

[2] A. Kojima, K. Teshima, Y. Shirai, T. Miyasaka, Organometal Halide Perovskites as Visible-Light Sensitizers for Photovoltaic Cells. Journal of the American Chemical Society, 131(17), (2009) 6050–6051. https://doi.org/10.1021/ja809598r

[3] M.A. Green, E.D. Dunlop, M. Yoshita, N. Kopidakis, K. Bothe, G. Siefer, X. Hao, J.Y. Jiang, Solar Cell Efficiency Tables (version 66). Progress in Photovoltaics Research and Applications, 33(7), (2025) 795–810. https://doi.org/10.1002/pip.3919

[4] M.A. Green, E. D. Dunlop, M. Yoshita, N. Kopidakis, K. Bothe, G. Siefer, X. Hao, J. Y. Jiang, Solar Cell Efficiency Tables (version 65). Progress in Photovoltaics Research and Applications, 33(1), (2025) 3–15. https://doi.org/10.1002/pip.3867

[5] Ł. Haryński, K. Trocki, S. Bykkam, G. Del Pozo, B. Romero, B. Bochentyn, D. Glowienka, Degradation of Perovskite Solar Cells: Insights from Accelerated Testing Versus Outdoor Aging in two Climate Zones. Solar Energy, 303, (2025) 114131. https://doi.org/10.1016/j.solener.2025.114131

[6] D. Zhang, D. Li, Y. Hu, A. Mei, H. Han, Degradation Pathways in Perovskite Solar Cells and How to Meet International Standards. Communications Materials, 3(1), (2022) 58. https://doi.org/10.1038/s43246-022-00281-z

[7] L. Duan, D. Walter, N. Chang, J. Bullock, D. Kang, S. P. Phang, K. Weber, T. White, D. Macdonald, K. Catchpole, H. Shen, Stability Challenges for the Commercialization of Perovskite–Silicon Tandem solar cells. Nature Reviews Materials, 8(4), (2023) 261–281. https://doi.org/10.1038/s41578-022-00521-1

[8] S.S. Dipta, M.A. Rahim, A. Uddin, Encapsulating Perovskite Solar Cells for Long-Term Stability and Prevention of Lead Toxicity. Applied Physics Reviews, 11(2), (2024) 021301. https://doi.org/10.1063/5.0197154

[9] Z. Liu, R. Lin, M. Wei, M. Yin, P. Wu, M. Li, L. Li, Y. Wang, G. Chen, V. Carnevali, L. Agosta, V. Slama, N. Lempesis, Z. Wang, M. Wang, Y. Deng, H. Luo, H. Gao, U. Rothlisberger, H. Tan, All-Perovskite Tandem Solar Cells Achieving >29% Efficiency with Improved (100) Orientation in Wide-Bandgap Perovskites. Nature Materials, 24(2), (2025) 252–259. https://doi.org/10.1038/s41563-024-02073-x

[10] K.T. Tanko, Z. Tian, S. Raga, H. Xie, E.A. Katz, M. Lira-Cantu, Stability and Reliability of Perovskite Photovoltaics: Are we there yet?. MRS Bulletin, 50(4), (2025) 512–525. https://doi.org/10.1557/s43577-025-00863-5

[11] G. M. Meheretu, A.K. Worku, M.T. Yihunie, R.K. Koech, G.A. Wubetu, The Recent Advancement of Outdoor Performance of Perovskite Photovoltaic Cells Technology. Heliyon, 10(17), (2024) e36710. https://doi.org/10.1016/j.heliyon.2024.e36710

[12] H. Meddeb, M. Götz-Köhler, N. Neugebohrn, U. Banik, N. Osterthun, O. Sergeev, D. Berends, C. Lattyak, K. Gehrke, M. Vehse, Tunable Photovoltaics: Adapting Solar Cell Technologies to Versatile Applications. Advanced Energy Materials, 12(28), (2022) 2200713. https://doi.org/10.1002/aenm.202200713

[13] X. Wang, Z. Chen, P. Guo, Z. Gao, C. Mu, Z. Lu, Perovskite-R1: A Domain-Specialized Large Language Model for Intelligent Discovery of Precursor Additives and Experimental Design. Communications Materials, 7(1), (2026) 86. https://doi.org/10.1038/s43246-026-01099-9

[14] J. Thiesbrummel, S. Shah, E. Gutierrez-Partida, F. Zu, F. Peña-Camargo, S. Zeiske, J. Diekmann, F. Ye, K. P. Peters, K.O. Brinkmann, P. Caprioglio, A. Dasgupta, S. Seo, F.A. Adeleye, J. Warby, Q. Jeangros, F. Lang, S. Zhang, S. Albrecht, M. Stolterfoht, Ion-Induced Field Screening as a Dominant Factor in Perovskite Solar Cell Operational Stability. Nature Energy, 9(6), (2024) 664–676. https://doi.org/10.1038/s41560-024-01487-w

[15] M.A. Green, E.D. Dunlop, M. Yoshita, N. Kopidakis, K. Bothe, G. Siefer, D. Hinken, M. Rauer, J. Hohl-Ebinger, X. Hao, Solar Cell Efficiency Tables (version 64). Progress in Photovoltaics Research and Applications, 32(7), (2024) 425–441. https://doi.org/10.1002/pip.3831

[16] M.A. Green, E.D. Dunlop, M. Yoshita, N. Kopidakis, K. Bothe, G. Siefer, X. Hao, Solar Cell Efficiency Tables (version 63). Progress in Photovoltaics Research and Applications, 32(1), (2023) 3–13. https://doi.org/10.1002/pip.3750

[17] Q. Jiang, K. Zhu, Rapid Advances Enabling High-Performance Inverted Perovskite Solar Cells. Nature Reviews Materials, 9(6), (2024) 399–419. https://doi.org/10.1038/s41578-024-00678-x

[18] H. Gao, K. Xiao, R. Lin, S. Zhao, W. Wang, S. Dayneko, C. Duan, C. Ji, H. Sun, A. D. Bui, C. Liu, J. Wen, W. Kong, H. Luo, X. Zheng, Z. Liu, H. Nguyen, J. Xie, L. Li, H. Tan, Homogeneous Crystallization and Buried Interface Passivation for Perovskite Tandem Solar Modules. Science, 383(6685), (2024) 855–859. https://doi.org/10.1126/science.adj6088

[19] C. Moon, C.H. Kim, J. Min, J. Koh, P. Boonmongkolras, G.K. Asare, F. Hollmann, H. H. Park, C.B. Park, B. Shin, Halide Perovskite Stabilized in a Photoelectrochemical Environment by Impermeable Single Crystal TiO_2 for Semi-Artificial Photosynthesis. Journal of Materials Chemistry A, 13(47), (2025) 40908–40918. https://doi.org/10.1039/d5ta05513j

[20] C.S. Pathak, H. Choi, H. Kim, J. Lim, S. Cho, D.S. Ham, S. Song, Recent progress in coating Methods for Large-Area Perovskite Solar Module Fabrication. Solar RRL, 8(4), (2023) 2300860. https://doi.org/10.1002/solr.202300860

[21] R.V. Babu, J.M. Fernandes, M. Kovendhan, N. Purushothamreddy, R. Muniramaiah, R. Arockiakumar, N. Karthiselva, D.P. Joseph,

Investigation of Structural, Optical, Electrical and Mechanical Properties of Transparent Conducting 'Ag' Electrodes. Physica B: Condensed Matter, 607, (2021) 412690. https://doi.org/10.1016/j.physb.2020.412690

[22] J. Li, H. Wang, X.Y. Chin, H. A. Dewi, K. Vergeer, T.W. Goh, J.W.M. Lim, J.H. Lew, K.P. Loh, C. Soci, T.C. Sum, H.J. Bolink, N. Mathews, S. Mhaisalkar, A. Bruno, Highly Efficient Thermally Co-Evaporated Perovskite Solar Cells and Mini-Modules. Joule, 4(5), (2020) 1035–1053. https://doi.org/10.1016/j.joule.2020.03.005

[23] M. Munjal, T. Prein, M.M. Ramadan, H.B. Smith, V. Venugopal, J. L. Rupp, I.I. Abate, E.A. Olivetti, K.J. Huang, Process Cost Analysis of Performance Challenges and their Mitigations in Sodium-Ion Battery Cathode Materials. Joule, 9(5), (2025) 101871. https://doi.org/10.1016/j.joule.2025.101871

[24] S. Huang, K. Tian, H. Huang, C. Li, W. Chu, K. Lee, Y. Huang, W. Su, Controlling the Morphology and Interface of the Perovskite Layer for Scalable High-Efficiency Solar Cells Fabricated using Green Solvents and Blade Coating in an Ambient Environment. ACS Applied Materials & Interfaces, 12(23), (2020) 26041–26049. https://doi.org/10.1021/acsami.0c06211

[25] P. Barua, N.K. Elumalai, A. Uddin, P. Sonar, K. Krishnan, Stability of Lead-Free Perovskite Solar Cells. Advanced Sustainable Systems, 10(3), (2026) e00008. https://doi.org/10.1002/adsu.202600008

[26] F. Jafarzadeh, L.A. Castriotta, E. Calabrò, P. Spinelli, A. Generosi, B. Paci, D.B. Rodriguez, M. Luce, A. Cricenti, F. Di Giacomo, F. Matteocci, F. Brunetti, A. Di Carlo, Stable and Sustainable Perovskite Solar Modules by optimizing blade coating Nickel Oxide Deposition over 15 × 15 cm^2 Area. Communications Materials, 5(1), (2024) 186. https://doi.org/10.1038/s43246-024-00576-3

[27] S. Yuan, D. Zheng, T. Zhang, Y. Wang, F. Qian, L. Wang, X. Li, H. Zheng, Z. Diao, P. Zhang, T. Pauporté, S. Li, Scalable Preparation of Perovskite Films with Homogeneous Structure via Immobilizing Strategy for High-Performance Solar Modules. Nature Communications, 16(1), (2025) 2052. https://doi.org/10.1038/s41467-025-57303-w

[28] M. Ma, C. Zhang, Y. Ma, W. Li, Y. Wang, S. Wu, C. Liu, Y. Mai, Efficient and Stable Perovskite Solar Cells and Modules Enabled by Tailoring Additive Distribution According to the Film Growth Dynamics. Nano-Micro Letters, 17(1), (2024) 39. https://doi.org/10.1007/s40820-024-01538-7

[29] H. Zhu, S. Teale, M.N. Lintangpradipto, S. Mahesh, B. Chen, M.D. McGehee, E.H. Sargent, O.M. Bakr, Long-Term Operating Stability in Perovskite Photovoltaics. Nature Reviews Materials, 8(9), (2023) 569–586. https://doi.org/10.1038/s41578-023-00582-w

[30] V. Paraskeva, M. Norton, A. Livera, A. Kyprianou, M. Hadjipanayi, E. Peraticos, A. Aguirre, S. Ramesh, T. Merckx, R. Ebner, T. Aernouts, A. Krishna, G.E. Georghiou, Diurnal Changes and Machine Learning Analysis of Perovskite Modules based on Two Years of Outdoor Monitoring. ACS Energy Letters, 9(10), (2024) 5081–5091. https://doi.org/10.1021/acsenergylett.4c01943

[31] Q. Emery, M. Remec, G. Paramasivam, S. Janke, J. Dagar, C. Ulbrich, R. Schlatmann, B. Stannowski, E. Unger, M. Khenkin, Encapsulation and Outdoor Testing of Perovskite Solar Cells: Comparing Industrially Relevant Process with a Simplified Lab Procedure. ACS Applied Materials & Interfaces, 14(4), (2022) 5159–5167. https://doi.org/10.1021/acsami.1c14720

[32] P. Mariani, M.Á. Molina-García, J. Barichello, M.I. Zappia, E. Magliano, L.A. Castriotta, L. Gabatel, S. B. Thorat, A.E. Del Rio Castillo, F. Drago, E. Leonardi, S. Pescetelli, L. Vesce, F. Di Giacomo, F. Matteocci, A. Agresti, N. De Giorgi, S. Bellani, A. Di Carlo, F. Bonaccorso, Low-Temperature Strain-Free Encapsulation for Perovskite Solar Cells and Modules Passing Multifaceted Accelerated Ageing Tests. Nature Communications, 15(1), (2024) 4552. https://doi.org/10.1038/s41467-024-48877-y

[33] G. Zhang, Y. Zheng, H. Wang, G. Ding, F. Yang, Y. Xu, J. Yu, Y. Shao, Shellac Protects Perovskite Solar Cell Modules under Real-World Conditions. Joule, 8(2), (2024) 496–508. https://doi.org/10.1016/j.joule.2023.12.008

[34] L. McGovern, E. C. Garnett, S. Veenstra, B. Van Der Zwaan, A Techno-Economic Perspective on Rigid and Flexible Perovskite Solar Modules. Sustainable Energy & Fuels, 7(21), (2023) 5259–5270. https://doi.org/10.1039/d3se00828b

[35] S. Iglesias-Porras, A. Neild, J. Gausden, M. Barraclough, E.A. Gibson, The Role of MAPbI3 Hydrate in Triple Mesoscopic Stack Minimodules: the Key to Elongating Outdoor lifespan. EES Solar, 1(4), (2025) 632–644. https://doi.org/10.1039/d5el00076a

[36] O. Nwafor, Integrated Photovoltaic Applications: Technological Advancements, Case Studies, Economic Viability, Policy Implications, and Environmental Impact. Solar Compass, 15, (2025) 100136. https://doi.org/10.1016/j.solcom.2025.100136

[37] V. Larini, C. Ding, F. Faini, G. Pica, G. Bruni, L. Pancini, S. Cavalli, M. Manzi, M. Degani, R. Pallotta, M. De Bastiani, C. Ma, G. Grancini, Sustainable and Circular Management of Perovskite Solar Cells Via Green Recycling of Electron Transport Layer-Coated Transparent Conductive Oxide. Advanced Functional Materials, 34(50), (2023) 2306040. https://doi.org/10.1002/adfm.202306040

[38] Y. Liu, Z. Zhang, T. Wu, W. Xiang, Z. Qin, X. Shen, Y. Peng, W. Shen, Y. Li, L. Han, Cost Effectivities Analysis of Perovskite Solar Cells: Will it Outperform Crystalline Silicon Ones? Nano-Micro Letters, 17(1), (2025) 219. https://doi.org/10.1007/s40820-025-01744-x

[39] M. U. Ali, H. Mo, Y. Li, A. B. Djurišić, Outdoor Stability Testing of Perovskite Solar Cells: Necessary Step Toward Real-Life Applications. APL Energy, 1(2), (2023). https://doi.org/10.1063/5.0155845

[40] P. Amalathas, S. Sunthareswaran, N. Neykova, L. Horák, J. Holovský, Stabilizing Halide Distribution in Mixed Halide Perovskites through Diammonium-Based Passivation. ACS Omega, 11(12), (2026) 19903–19913. https://doi.org/10.1021/acsomega.6c01620

[41] C. Boyd, R. Cheacharoen, K. A. Bush, R. Prasanna, T. Leijtens, M. D. McGehee, Barrier Design to Prevent Metal-Induced Degradation and Improve Thermal Stability in Perovskite Solar Cells. ACS Energy Letters, 3(7), (2018) 1772–1778. https://doi.org/10.1021/acsenergylett.8b00926

[42] F. Baumann, S. R. Raga, M. Lira-Cantú, Monitoring the Stability and Degradation Mechanisms of Perovskite Solar Cells by in Situ and Operando Characterization. APL Energy, 1(1), (2023). https://doi.org/10.1063/5.0145199

[43] P. Kore, M. Jamshidi, J. M. Gardner, The Impact of Moisture on the Stability and Degradation of Perovskites in Solar Cells. Materials Advances, 5(6), (2024) 2200–2217. https://doi.org/10.1039/d3ma00828b

[44] Hussain, A. Bibi, M.I.K. Khail, T. Zhenbo, R. Khan, Z. Hussain, F. Yu, C.Z. Zao, M.K. Khan, Advancing Environmental Remediation: Mechanistic Insights into SnO_2-based Photocatalysts for Organic Pollutant Degradation and Microbial Inactivation. Journal of Water Process Engineering, 77, (2025) 108511. https://doi.org/10.1016/j.jwpe.2025.108511

[45] U. Erdil, M. Khenkin, M. Remec, Q. Emery, V. Sudhakar, R. Schlatmann, A. Abate, E. A. Katz, C. Ulbrich, Mimicking Outdoor ion Migration in Perovskite Solar Cells: A Forward Bias, No-Light Accelerated Aging Approach. ACS Energy Letters, 10(3), (2025) 1529–1537. https://doi.org/10.1021/acsenergylett.5c00376

[46] R.K. Gupta, I. Visoly-Fisher, Temperature effects on Diurnal Metastability of Perovskite Solar Cells. APL Energy, 4(1), (2026) 010901. https://doi.org/10.1063/5.0319232

[47] B. Guo, M. Chauhan, N. R. Woodward, G. R. McAndrews, G. J. Thapa, B. M. Lefler, R. Li, T. Wang, K. Darabi, M. D. McGehee, A. Amassian, In situ stress monitoring reveals tension and wrinkling evolutions during halide perovskite film formation. ACS Energy Letters, 9(1), (2023) 75–84. https://doi.org/10.1021/acsenergylett.3c02079

[48] L. Zhang, D. Liu, G. Du, L. Cai, W. Dai, Y. Dong, H. Dai, Y. Gong, S. Zhang, B. Yan, J. Yao, Report on the relevance of Perovskite Module Outdoor ageing Performance and Indoor UV Degradation Trend. Nanoscale Advances, 7(19), (2025) 6248–6256. https://doi.org/10.1039/d5na00622h

[49] F. Cao, L. Bian, L. Li, Perovskite Solar Cells with High-Efficiency Exceeding 25%: A review. Energy Materials and Devices, 2(1), (2024) 9370018. https://doi.org/10.26599/emd.2024.9370018

[50] T. R. Rana, M. Abbas, E. Schwartz, F. Jiang, M. Y. Yaman, Z. Xu, D. S. Ginger, D. MacKenzie, Scalable Passivation Strategies to Improve Efficiency of Slot Die-Coated Perovskite Solar Cells. ACS Energy Letters, 9(4), (2024) 1888–1894. https://doi.org/10.1021/acsenergylett.4c00651

[51] Y. Zhu, Y. Zhang, M. Hu, L. Wan, W. Huang, J. Chu, Y. Hao, Y. Cheng, A.N. Simonov, J. Lu, Scalable Slot-Die Coating of Passivation Layers for Improved Performance of Perovskite Solar Cell Modules. Small Methods, 9(4), (2024) e2401244. https://doi.org/10.1002/smtd.202401244

[52] Z. Hu, Z.Wang, P. Gao, Advancements in Scaling Up Perovskite Solar Cells: from Small-Area Devices to Large-Scale Modules. ChemPhysChem, *25*(22), (2024) e202400587. https://doi.org/10.1002/cphc.202400587

[53] V. C. M. Duarte, L. Andrade, Recent Advancements on Slot-Die Coating of Perovskite Solar Cells: The lab-to-fab optimisation process. Energies, 17(16), (2024) 3896. https://doi.org/10.3390/en17163896

[54] Y. Y. Kim, T. Yang, R. Suhonen, A. Kemppainen, K. Hwang, N. J. Jeon, J. Seo, Roll-to-roll gravure-Printed Flexible Perovskite Solar Cells using eco-friendly Antisolvent Bathing with Wide Processing Window. Nature Communications, 11(1), (2020) 5146. https://doi.org/10.1038/s41467-020-18940-5

[55] Y. Jeong, Y. Kim, H. Lee, S. Ko, S.S. Ham, H.R. Jung, J.H. Choi, W.M. Kim, J. Jeong, S. Yoon, D. J. Hwang, G.Y. Kim, Laser Scribing for Perovskite Solar Modules of Long-Term Stability. Solar RRL, 8(8), (2024) 2301040. https://doi.org/10.1002/solr.202301040

[56] E.R. Soto, V.C.M. Duarte, A. Mendes, L. Andrade, Inverted Perovskite Solar Modules with 99.3% Geometrical Fill Factor via Nanosecond Single Laser Patterning. Communications Engineering, 4(1), (2025) 198. https://doi.org/10.1038/s44172-025-00512-4

[57] A. Kang, F. Yan, Emerging Strategies for the Large-Scale Fabrication of Perovskite Solar Modules: From design to process. Energy & Environmental Science, 18(9), (2025) 3917–3954. https://doi.org/10.1039/d4ee05613b

[58] J.H. Park, S. Hwang, A Polyolefin Elastomer Encapsulant Modified by an Ethylene–Propylene–Diene Terpolymer for Photovoltaic Applications. ACS Omega, 9(3), (2024) 3858–3865. https://doi.org/10.1021/acsomega.3c07969

[59] W. Post, M. Kersemans, I. Solodov, K. Van Den Abeele, S. García, S. Van Der Zwaag, Non-Destructive Monitoring of Delamination Healing of a CFRP Composite with a Thermoplastic Ionomer Interlayer. Composites Part a Applied Science and Manufacturing, 101, (2017) 243–253. https://doi.org/10.1016/j.compositesa.2017.06.018

[60] M. V. Khenkin, E.A. Katz, A. Abate, G. Bardizza, J. J. Berry, C. Brabec, F. Brunetti, V. Bulović, Q. Burlingame, A. Di Carlo, R. Cheacharoen, Y. Cheng, A. Colsmann, S. Cros, K. Domanski, M. Dusza, C.J. Fell, S.R. Forrest, Y. Galagan, M. Lira-Cantu, Consensus Statement for Stability Assessment and Reporting for Perovskite photovoltaics based on ISOS Procedures. Nature Energy, 5(1), (2020) 35–49. https://doi.org/10.1038/s41560-019-0529-5

[61] J. Chakar, U. Erdil, A. Burgaud, M. Remec, A. Abate, C. Ulbrich, R. Schlatmann, Y. Bonnassieux, M. Khenkin, J. Puel, Bridging Accelerated Indoor Aging and Outdoor Stability of Perovskite Solar Cells using a Bayesian Modeling Framework. Solar RRL, 9(24), (2025) e202500716. https://doi.org/10.1002/solr.202500716

[62] K. Weiß, E. Klimm, I. Kaaya, Accelerated aging tests vs field performance of PV modules. Progress in Energy, 4(4), (2022) 042009. https://doi.org/10.1088/2516-1083/ac890a

[63] C.E. Torrence, C.S. Libby, W. Nie, J.S. Stein, Environmental and Health Risks of Perovskite Solar Modules: Case for Better Test Standards and Risk Mitigation Solutions. iScience, 26(1), (2022) 105807. https://doi.org/10.1016/j.isci.2022.105807

[64] W.E. Latchiba, S. Waita, R. Krueger, J.M. Mwabora, Assessment of the Life Cycle of Photovoltaic Solar Technologies for Sustainable Energy Transitions: Implications for Climate Policy and Low-Carbon System Integration. Resources Environment and Sustainability, 25, (2026) 100328. https://doi.org/10.1016/j.resenv.2026.100328

[65] X. Tian, S.D. Stranks, F. You, Life cycle assessment of recycling strategies for perovskite photovoltaic modules. Nature Sustainability, 4(9), (2021) 821–829. https://doi.org/10.1038/s41893-021-00737-z

[66] J.J. Cordell, M. Woodhouse, E.L. Warren, Technoeconomic Analysis of Perovskite/Silicon Tandem Solar Modules. Joule, 9(2), (2025) 101781. https://doi.org/10.1016/j.joule.2024.10.013

Authors Contribution Statement

B. Punithaveni: Investigation, Resources, Writing - Original Draft. D. Nithyaprakash: Conceptualization, Validation, Writing - Review & Editing. Mohanbabu Bharathi: Resources, Writing - Review & Editing. All authors read and approved the final manuscript.

Funding

The authors declare that no funds, grants or any other support were received during the preparation of this manuscript.

Competing Interests

The authors declare that there are no conflicts of interest regarding the publication of this manuscript.

Generative AI Declaration

ChatGPT (GPT-5) was used only for English language improvement and content polishing. All scientific content, interpretations, and conclusions were developed and verified by the authors, who take full responsibility for the manuscript.

Data Availability

No new data were generated or analyzed in this study. All information discussed in this review is available within the manuscript and in the cited references.

Has this article screened for similarity?

Yes